Title
Variation in the Holton–Tan effect by longitude

Permalink
https://escholarship.org/uc/item/35z537nb

Journal
Quarterly Journal of the Royal Meteorological Society, 147(736)

ISSN
0035-9009

Authors
Elsbury, Dillon
Peings, Yannick
Magnusdottir, Gudrun

Publication Date
2021-04-01

DOI
10.1002/qj.3993

Copyright Information

Peer reviewed

RESEARCH ARTICLE

Variation in the Holton–Tan effect by longitude

Dillon Elsbury | **Yannick Peings** | **Gudrun Magnusdottir**

Department of Earth System Science,
University of California, Irvine, California

Correspondence
D. Elsbury, Department of Earth System
Science, University of California Irvine,
Irvine, CA 92617, USA
Email: delsbury@uci.edu

Present Address
D. Elsbury, Department of Earth System
Science, University of California Irvine,
Irvine, California 92617, United States of
America

Abstract

The teleconnection between the Quasi-Biennial Oscillation (QBO) and the boreal winter polar vortex, the Holton–Tan effect, is analyzed in the Whole Atmosphere Community Climate Model (WACCM) with a focus on how stationary wave propagation varies by QBO phase. These signals are difficult to isolate in reanalyses because of large internal variability in short observational records, especially when decomposing the data by QBO phase. A 1,500-year ensemble is leveraged by defining the QBO index at five different isobars between 10 and 70 hPa. The Holton–Tan effect is a robust part of the atmospheric response to the QBO in WACCM with warming of the polar stratosphere during easterly QBO (QBOE). A nudging technique is used to reduce polar stratospheric variability in one simulation. This enables isolation of the impact of the QBO on the atmosphere in the absence of a polar stratospheric response to the QBO: referred to as the "direct effect" and the polar stratospheric response, "indirect effect." This simulation reveals that the polar stratospheric warming during QBOE pushes the tropospheric jet equatorward, opposing the poleward shift of the jet by the QBOE, especially over the North Pacific. The Holton–Tan effect varies over longitude. The QBO induces stronger planetary wave forcing to the mean flow in the extratropical lower stratosphere between Indonesia and Alaska. The North Pacific polar stratosphere responds to this before other longitudes. What follows is a shift in the position of the polar vortex toward Eurasia (North America) during easterly (westerly) QBO. This initiates downstream planetary wave responses over North America, the North Atlantic, and Siberia. This spatiotemporal evolution is found in transient simulations in which QBO nudging is "switched on." The North Pacific lower stratosphere seems more intrinsically linked to the QBO while other longitudes appear more dependent on the mutual interaction between the QBO and polar stratosphere.

KEYWORDS
Holton–Tan effect, Quasi-Biennial Oscillation, stratosphere–troposphere coupling, stratospheric polar vortex

1 | INTRODUCTION

Alternating easterly and westerly winds descend through the tropical stratosphere with an averaged periodicity of roughly 28 months, while both longer (35 months) and shorter (22 months) periods have been observed (Bushell *et al.*, 2020). This variability is called the Quasi-Biennial Oscillation (QBO). While the QBO is located in the tropics, it has effects on global-scale circulation (Gray *et al.*, 2018). One of these teleconnections is the so-called Holton–Tan effect: when QBO easterlies (QBOE) are located in lower tropical stratosphere, the polar vortex that forms during boreal winter is weaker than its climatological average. Conversely, the circumpolar westerlies making up the polar vortex are stronger when QBO westerlies are present in the tropical lower stratosphere (QBOW). Our knowledge on this teleconnection continues to progress (Holton and Tan, 1980; Lu *et al.*, 2020). However, how the teleconnection varies over longitude, apart from the conventional zonal mean, is less frequently shown. This work aims to close this gap in our knowledge.

Stationary planetary scale waves propagate upward and equatorward through the stratosphere during boreal winter (Matsuno, 1970). Per the classic Holton–Tan mechanism, these waves are confined farther north because the stratospheric zero wind line flanking the QBO is at a more northern latitude when it is QBOE rather than QBOW; the zero-wind line is in the southern hemisphere during QBOW (Holton and Tan, 1980; Andrews *et al.*, 2019). Therefore, more wave breaking occurs along the polar vortex during QBOE than during QBOW in early winter (Lu *et al.*, 2020). The Holton–Tan effect is found in reanalysis data (Holton and Tan, 1980; 1982; Dunkerton and Baldwin, 1991; Gray *et al.*, 2001b; Lu *et al.*, 2008; Naoe and Shibata, 2010; Yamashita *et al.*, 2011; Anstey and Shepherd, 2014; Lu *et al.*, 2014; White *et al.*, 2015; Lu *et al.*, 2020) and in idealized model simulations (Gray *et al.*, 2001a; Gray *et al.*, 2003; Naito and Yoden, 2006; Yamashita *et al.*, 2011; Garfinkel *et al.*, 2012; Rao *et al.*, 2020).

The importance of the zero-wind line effect versus that of the QBO implicit meridional circulation (QBO-MMC) in causing the Holton–Tan effect has been debated (Garfinkel *et al.*, 2012). For schematics and discussion of the QBO-MMC see Plumb and Bell(1982) and Collimore *et al.* (2003). During QBOE and QBOW, the tropical lower stratosphere cools and warms, respectively. Consistent with this cooling during QBOE is adiabatic expansion, upward motion through the tropical stratosphere that is complemented by poleward diverging flow into the extratropics, sinking motion, and an equatorward return flow in the lower stratosphere (Garfinkel and Hartmann, 2011a).

The regions of ascent and descent coincide with cooling and warming, respectively. Therefore, the tropical lower stratospheric cooling taking place during QBOE coincides with lower stratospheric warming in the extratropics. The opposite circulation occurs during QBOW so that the tropical lower stratosphere is warmer than expected by climatology, while the extratropical lower stratosphere is cooler. The meridional and vertical extent of the QBO-MMC varies by season, and it is modulated by forcing due to extratropical wave breaking. The strength of the circulation generally decreases with height in the stratosphere, and its meridional extent, which extends farther poleward in the winter hemisphere, has been shown to reach 40°N to 50°N during boreal winter in reanalysis (Kinnersley, 1999; Huesmann and Hitchman, 2001; Peña-Ortiz *et al.*, 2008; Coy *et al.*, 2016).

The QBO-MMC is intrinsically linked to the stratospheric wave guide and affects where stationary waves may propagate. It affects the climatological equatorward propagation of these waves between ~20–5 hPa. This is thought to result in more wave breaking in the subpolar upper stratosphere during QBOE (Ruzmaikin *et al.*, 2005; Garfinkel *et al.*, 2012; Lu *et al.*, 2014; Rao *et al.*, 2020). The QBO-MMC also shifts the tropospheric jet poleward during QBOE, an additional effect on the waveguide (White *et al.*, 2015). As many of the studies investigating the Holton–Tan effect use zonal mean analyses, it is not clear how the Holton–Tan effect and associated mechanisms vary over longitude.

Zonal asymmetry in the Holton–Tan effect may exist for a number of reasons. The QBO and QBO-MMC promote regional changes in the extratropical circulation that vary throughout the winter season (Chen and Li, 2007; Garfinkel and Hartmann, 2010; Garfinkel and Hartmann, 2011a; 2011b; Gray *et al.*, 2018). These responses may constructively interfere (Fletcher and Kushner, 2011) with the climatological stationary wave pattern originating from orography, land sea contrast, and ocean heat fluxes (Garfinkel *et al.*, 2020), promoting upward wave activity that then affects the polar stratosphere. The QBO and QBO-MMC may also promote regional changes in wave activity by acting on synoptic scale eddies over the ocean basins. They have a robust impact on these waves near the extratropical tropopause, a feature found in reanalysis and model simulations (Garfinkel and Hartmann, 2011a; 2011b; White *et al.*, 2016; Wang *et al.*, 2018). Synoptic scale waves interact with the lower frequency mean flow, blocks, and stationary wave trains included (Nakamura *et al.*, 1997; Lorenz and Hartmann, 2001; 2003; Eichelberger and Hartmann, 2007) and thus may affect stationary waves. So, perhaps interaction between waves of various scales is necessary for

changes in wave activity (e.g., Boljka and Birner, 2020). A final hypothesis is that zonal asymmetry in the QBO teleconnection arises because the QBO itself is zonally asymmetric (Hitchman and Huesmann, 2009; Tegtmeier *et al.*, 2020). Should the intrinsic qualities of the QBO control its meridional extent (Haynes, 1998), perhaps this proximately controls the meridional extent of the QBO-MMC. This would then affect where extratropical planetary scale wave breaking takes place in the stratosphere.

Looking for zonal asymmetry requires a large ensemble of data to limit the influence of internal variability and extract the QBO effect. This is especially limiting in reanalyses when decomposing between easterly and westerly QBO years leads to about 20 years of data for each, a small sample in regards to the highly variable northern hemisphere atmospheric circulation in winter. In this study, we take advantage of a 1,500-year set of simulations performed with the Whole Atmosphere Community Climate Model version 4 (WACCM) to explore the QBO teleconnections with robustness. We focus on three key aspects of the problem:

1. How does the extratropical response evolve with the QBO cycle? Instead of defining the QBO at one specific pressure level in the atmosphere, we will define it at five levels, examining how the extratropical atmosphere responds to the QBO during each phase of its cycle. This is made possible by the large ensemble of simulations that allows for sufficient sample sizes even after decomposing between QBO at different levels (from 10 to 70 hPa).
2. How does the QBO effect vary over longitude? We will investigate how the QBO influences stationary planetary scale waves in specific sectors: the North Atlantic (45°W to 45°E), over Siberia (45°E to 135°E), the North Pacific (135°E to 135°W), and over North America (135°W to 45°W).
3. What is the impact of the QBO on the extratropical atmosphere versus that from polar stratospheric variability? For this, we will use a nudging technique to turn off the polar stratospheric feedback to the QBO in the model (the Holton–Tan effect). This isolates a more direct atmospheric response to the QBO that we refer to as the "direct effect" in this article, which will be contrasted with the "indirect effect," the latter being the variability of the Holton–Tan effect.

Methods follow this section, results will be presented in the third section, and we end with discussion and conclusions in the fourth section.

2 | METHODS

2.1 | Model

The Atmospheric General Circulation Model (AGCM) used in this study is the Whole Atmosphere Community Climate Model (WACCM, Marsh *et al.*, 2013) with CAM4 physics and the specified chemistry option (referred to as SC-WACCM4, Smith *et al.*, 2014). The specified chemistry decreases the computational cost of the model while retaining comparable climatology with the standard version. This is the main motivation for using specified chemistry since in this particular study we prioritize large ensemble size to model complexity. The model domain extends from the surface to 5.1×10^{-6} hPa, ~145 km with 66 vertical levels and a horizontal resolution of 1.9° latitude by 2.5° longitude. SC-WACCM4 does not simulate a QBO, but it includes an option to prescribe it by nudging the equatorial winds between 22°S and 22°N, from 86 to 4 hPa. The climatological 28-month QBO cycle derived from radiosonde data is imposed in the model (Matthes *et al.*, 2010), allowing us to explore its influence on the extratropical circulation.

2.2 | Control simulation

The control (CTL) simulation consists of a concatenation of five 300-member simulations forced with the 1979–2008 average annual cycle of present-day sea-surface temperature (derived from HadISST data, Rayner *et al.*, 2003). The external forcings (greenhouse gases, aerosols, volcanoes) are set to their 2000 value. Each ensemble member is started on April 1 and ends after the completion of May 31 of the following year. The first April and May are discarded for spin-up, leaving one full year of simulation for each member. The five different simulations only differ by their treatment of Arctic sea ice. These experiments are part of the Polar Amplification Model Intercomparison Project (PAMIP), which aims to investigate polar-mid-latitude linkages (Smith *et al.*, 2019). They include the following sea ice concentration (SIC) and sea ice thickness (SIT) forcings: (a) present-day SIC (1979–2008 average annual cycle) with fixed 2 m SIT, (b) preindustrial SIC (derived from preindustrial CMIP5 control runs) with fixed 2 m SIT, (c) future SIC (derived from RCP8.5 CMIP5 runs) with fixed 2 m SIT, (d) present-day SIC with spatially varying SIT (1979–2008 average annual cycle from PIOMAS, Zhang and Rothrock, 2003), and (e) future SIC with future SIT (also derived from RCP8.5 CMIP5 runs). Details on the experimental design are given in Smith *et al.* (2019). The

assumption we make is that if robust in our model, the Holton–Tan effect should not be too dependent on the state of Arctic sea ice. We have verified that this is indeed the case (Figure S1), and therefore concatenate the five runs to obtain a valuable ensemble of 1,500 years, which allows for highly robust results.

Each of the ensemble members is initialized with a different month in the QBO cycle. For instance, member one is forced starting with the first month of the 28-month QBO cycle, while member two is forced starting with month two of the 28-month QBO cycle, and so on. Thus, with a 28-month cycle and 1,500 ensemble members, each month of the QBO cycle is used to initialize about 50 members. This deliberate "walking down" of the QBO ensures that there will be variability in the QBO cycle among members, allowing us to composite them based on the phase of the QBO. Note that the transient response to the QBO is diagnosed. Following Garfinkel and Hartmann, 2011b, this is more pertinent to studying the observed response to the QBO than a multi-year response. A multi-year equilibrated response would be conflated with a response to the QBO, but also with subtropical stratospheric "memory" that could influence planetary wave propagation (Scott and Haynes, 1998).

2.3 | Climatological polar stratosphere experiment

An additional simulation, Climatological Polar Stratosphere (CPS), is used to isolate the tropospheric response to the QBO from the polar stratospheric response. It is forced with the 1979–2008 average annual cycle of SST/SIC and the same prescribed QBO. The polar stratospheric variability in CPS is suppressed by nudging the atmospheric circulation in the polar stratosphere towards its climatology. This prevents the propagation of waves into the polar stratosphere and reveals the tropospheric response to the QBO in the absence of the polar stratosphere response.

To implement the nudging, a reference 3-hr climatology is created from simulation (1) in the aforementioned list of five simulations. The prognostic equations for temperature, zonal wind, and meridional wind of the polar stratosphere (north of 65°N and above 200 hPa) are nudged toward the reference climatology at every 30-min time step of the SC-WACCM4 run. The strength of the nudging, corresponding to a specific rate of Newtonian relaxation, is prescribed so that the atmosphere is fully constrained toward the target state every 2.5 hrs. This allows the model simulation to exhibit some internal variability while ensuring that climatological polar stratospheric winds and temperature field between the CTL and CPS simulations are

similar (Figure S2). A more thorough description of this nudging of the polar stratosphere towards climatology can be found in the supporting information of Peings (2019).

2.4 | Transient QBO response simulations

Three additional simulations are run to analyze the transient atmospheric response to the QBO. We run a 100-year control simulation with present-day-fixed SST/SIC variability and do not prescribe the QBO cycle. We then branch from November 1 of each year while imposing the QBO nudging and running the model through January 31. Two sets of branched runs are performed, one in which the tropical stratosphere is nudged toward QBOW, and another toward QBOE. Additional information on these simulations will be provided in section 3e.

2.5 | Diagnostic tools

The QBO is indexed at different isobars (10, 20, 30, 50, and 70 hPa) to show the dependency of the results on QBO phase, similar to indexing used by Huesmann and Hitchman (2001) for instance. The index is made from the area weighted, meridionally and zonally averaged, December and January zonal winds between 5°S and 5°N at the designated isobaric surface. We choose these two months because this is when the Holton–Tan effect is known to be active (Lu $et\ al.$, 2014; White $et\ al.$, 2015; Lu $et\ al.$, 2020). The sequential December and January periods are averaged together, and the lowest tercile of averaged wind speeds is used to define the easterly QBO indices. We refer to configurations of the QBO by what isobar the QBO is easterly at. So, QBO_{10} means easterlies are located at 10 hPa, QBO_{20} at 20 hPa, and so on (Figure 1). Judging by the winds in the lower stratosphere, QBO_{10} is our most westerly QBO (QBOW) state and QBO_{50} is a prototypical easterly QBO state (QBOE). QBO_{10} and QBO_{20} feature a waning lower stratospheric QBOW (Figure 1a,b), QBO_{30} features a nascent lower stratospheric QBOE (Figure 1c), and QBO_{50} and QBO_{70} prominent lower stratospheric QBOE (Figure 1d,e).

Every plot will show anomalies: anomalies during an individual month or day are calculated as deviations from that month's (e.g., December or January) or day's climatology. So, in the case of the 1,500-year control, we have an array of 3,000 anomalies for each grid point. The sequential December and January anomalies are averaged together, yielding an array of 1,500 DJ anomalies. Using the QBO_{50} index, for example, the indices corresponding to the easterly tercile of data (495 timesteps) are selected from this

CTL DJ Zonal Mean Response
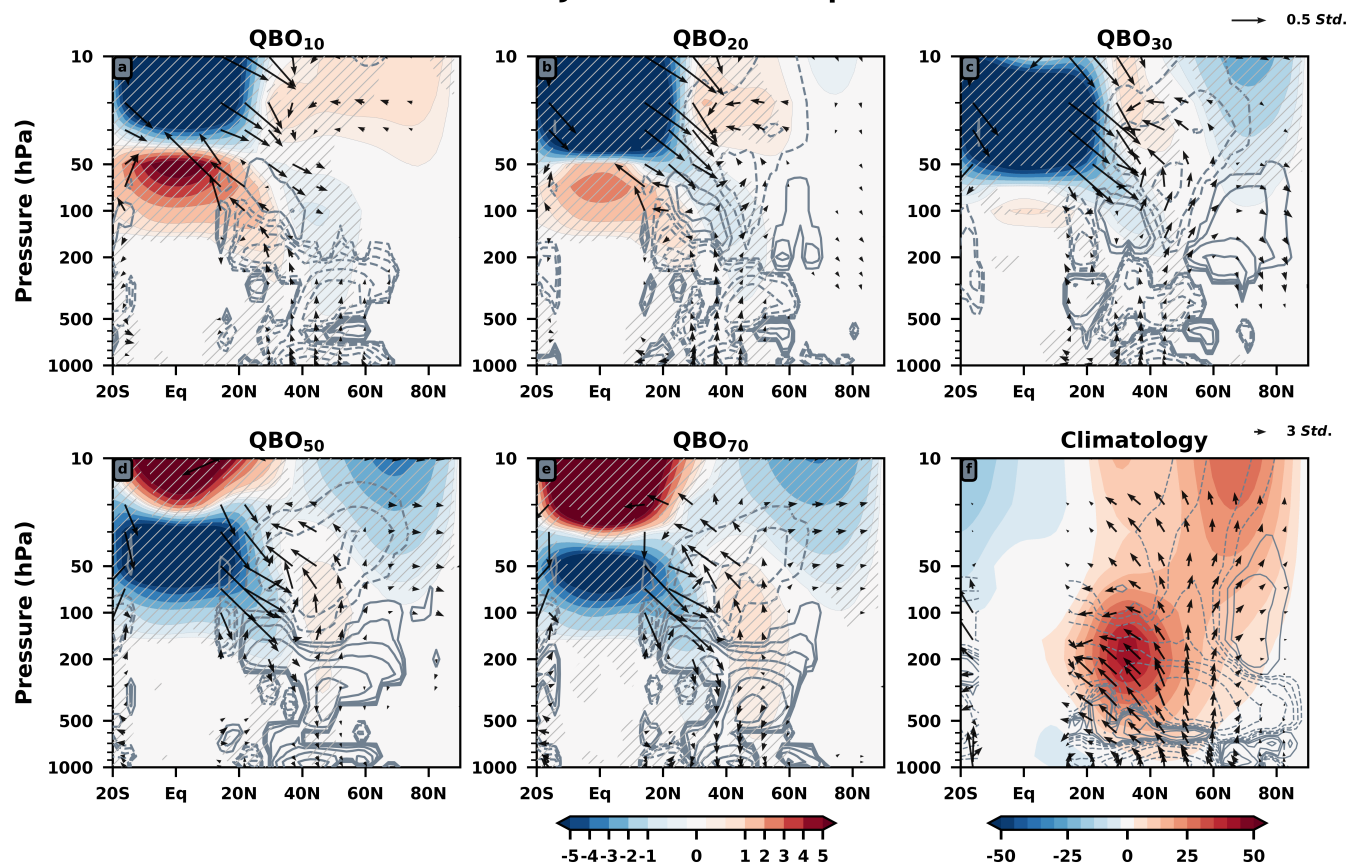
FIGURE 1 December and January (DJ) zonal mean responses to each of the five QBO indices. The isobar used to index the QBO is in the title of each composite. Zonal wind anomalies are shaded, and extra contour levels are used about zero to show the tropospheric wind response: Gray hatching is used to denote statistical significance. Wave activity flux (WAF) divergence is shown in black contours with intervals of +/ .001, .0025, .005, .01, .025, .05, .1, .25, .5 m·s^{-1}·day^{-1}. Standardized (by climatological standard deviation) vertical and meridional WAF responses are shown as vectors. Only statistically significant responses are shown for all fields other than zonal wind. Figure 1f shows the climatological response: Zonal wind is shaded, WAF divergence is shown similarly with intervals of +/ .01, .025, .05, .1, .25, .5, 1, 2.5, 5 m·s^{-1}·day^{-1}, and WAF vectors are instead shown as gray [Colour figure can be viewed at wileyonlinelibrary.com]

array. Then, those 495 timesteps are averaged together, yielding one composite, which shows how the atmosphere deviates from its climatologically averaged state when QBO easterlies are located at 50 hPa. All anomalies shown are responses to the QBO.

This is important when comparing CTL and CPS responses. If CTL and CPS are compared one to one, then biases in zonal wind emerge in the mid-latitude stratosphere because CPS breaks the Brewer–Dobson circulation, as it does not allow planetary waves to alter the mean flow in the polar stratosphere (Figure S2). CTL and CPS cannot be compared this way. Instead, anomalies are calculated with respect to QBO phase (as described above) in both CTL and CPS individually (Figure S3). By comparing these anomalous responses to the QBO between the simulations (CTL–CPS), polar stratospheric variability during a specific QBO phase can be estimated (Figure S3e–f).

A two-sided Student's t test is used to calculate significance: anomalies corresponding to the easterly QBO indices (~33% of the anomalies, 495 timesteps) are compared to the remaining ~67% of the anomalies (1,005 timesteps).

Anomalies and statistical significance are calculated this way for every figure except Figures 9 and 10. Methods used to create those figures will be described in later text.

The 3D wave activity flux of Plumb (1985, equation 5.7) is used throughout. When zonally averaged, it reduces to the Eliassen–Palm flux (Edmon *et al.*, 1980). The zonal, meridional, and vertical components are used to calculate the WAF divergence, which indicates where wave generation or dissipation is taking place (Plumb, 1985). The WAF is calculated using waves 1–3 as inputs for all analyses in the manuscript. The contribution of waves four and up is found to be small and is not included.

TABLE 1 The number of DJ periods making up each of the QBO indices are shown.

	10 hPa	20 hPa	30 hPa	50 hPa	70 hPa
10 hPa	**495**	382	145	1	0
20 hPa	382	**495**	258	87	0
30 hPa	145	258	**495**	324	142
50 hPa	1	87	324	**495**	313
70 hPa	0	0	142	313	**495**

Note: Cells off of the diagonal show the number of DJ periods overlapping between QBO indices. For example, 382 of the 495 DJ periods making the up the QBO 10 hPa index overlap with the QBO 20 hPa index.

3 | RESULTS

3.1 | QBO indexing scheme and Holton–Tan effect

We first examine the zonal mean zonal wind response to the QBO to see whether or not the CTL reproduces the Holton–Tan effect. Figure 1 shows this response with wave activity flux vectors and divergence overlaid.

Each frame in Figure 1 is composited using a different isobar to index the QBO (10 hPa for Figure 1a, 20 hPa for Figure 1b, and so on), and recall that we exclusively focus on the easterly tercile of data. In other words, instead of differentiating between QBOE/QBOW at a fixed level, henceforth, we will focus on QBOE at different pressure levels.

Ensemble members tend to overlap between adjacent QBO indices (Table 1). For instance, 382 of the 495 December and January periods making up the QBO_{10} index are also in the QBO_{20} index. Regardless of this overlap, composites created using different QBO indices contain unique features, showing that the background atmospheric state is sensitive to which isobar is chosen to define the QBO index.

Consistent with the Holton–Tan effect, the polar vortex is weaker while QBOE occupies the lower tropical stratosphere (Figures 1d,e). Conversely, the vortex is stronger (Figure 1a) than expected by climatology when the lower stratosphere features a prominent QBOW. Since this result is based on an average of 495 DJ seasons, it corroborates that the Holton–Tan effect is a robust part of the atmospheric response to the QBO in SC-WACCM4 (as previously shown in Zhang *et al.*, 2019). These zonal wind results are consistent with ERA5 reanalysis (Figure S4) from the European Centre for Medium-Range Weather Forecasts (Hersbach *et al.*, 2020). Note that the significant wave activity flux anomalies of Figure S4, are scant, underlining why we evaluate this field in SC-WACCM4.

TABLE 2 SSWs are subsampled by QBO phase using the 300 year present day SST/SIC dataset. Following from the tercile QBO indexing, 100 years of data is available per QBO index to check for SSWs. The total number of SSWs per QBO index is given along the diagonal. DJ is used to define to the QBO phase, while Nov. to Mar. is used to check for SSWs.

	10 hPa	20 hPa	30 hPa	50 hPa	70 hPa
10 hPa	**46**	27	13	0	0
20 hPa	27	**49**	27	8	0
30 hPa	13	27	**60**	29	17
50 hPa	0	8	29	**81**	50
70 hPa	0	0	17	50	**78**

Note: Cells of of the diagonal show the number of SSWs overlapping between QBO indices.

As an additional metric to quantify how the polar cap changes by QBO phase, we calculate the number of SSWs per QBO phase in the 300-year simulation set with prescribed present-day climatological SST and SIC. We continue to index the QBO based solely on December–January. Using the same tercile indexing method, 100 members are analyzed for each QBO background state. We use the algorithm of Charlton and Polvani (2007), analyzing U10 at 60°N from November 1 to March 31, excluding final warmings. These results (Table 2) reinforce the points above and show that the vortex is most disturbed during $QBO_{30\text{-}50\text{-}70}$, during which 60, 81, and 78 SSWs occur, respectively, per 100 years. QBO_{10} and QBO_{20} feature 46 and 49 SSWs, respectively. Across all 300 years, there are 168 SSWs, a frequency of 0.56 events per season, lower than the climatological average, which is just over six events per decade (Butler *et al.*, 2017).

During QBO_{10}, in the troposphere the equatorward portion of the subtropical jet strengthens while its poleward portion weakens (Figure 1a). The opposite set of anomalies is found during $QBO_{50\text{-}70}$. The arching of the zonal mean zonal wind anomalies out of the subtropical stratosphere is a response to the QBO-MMC. It modifies the eddy momentum flux due to transient eddies in the lower subtropical stratosphere (Garfinkel and Hartmann, 2011a; 2011b; Wang *et al.*, 2018). While the tropospheric wind anomalies are small, recall that the five different sea ice forcings result in unique tropospheric stationary wave responses, muddying the tropospheric response to the QBO (Figure S1, Appendix S1). This suggests that the tropospheric response to the QBO is robust. Nonetheless, these are zonal mean composites that mask sector-specific processes.
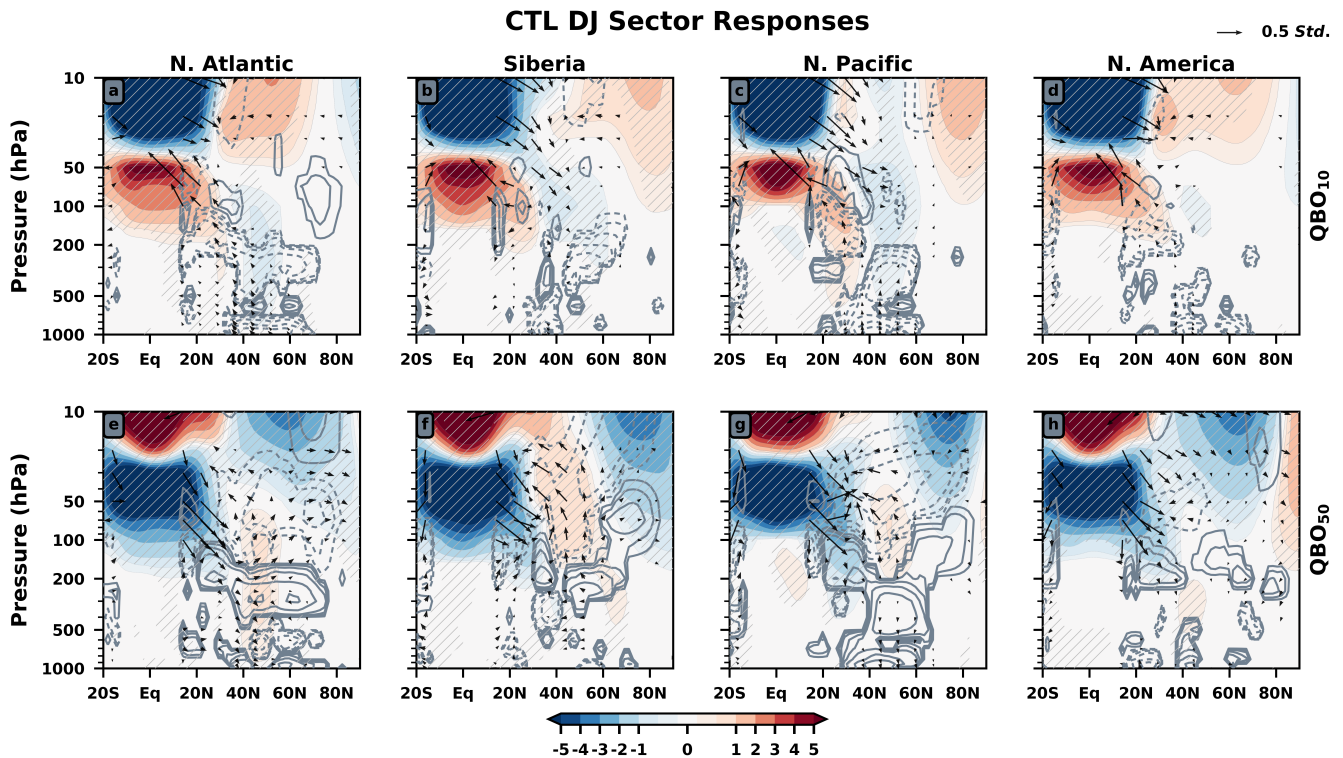
FIGURE 2 Zonally averaged anomalies of each longitudinal sector are shown with the same graphical convections used to create Figure 1. The columns from left to right show the North Atlantic (defined 45°W to 45°E), Siberia (45°E to 135°E), North Pacific (135°E to 135°W), and North America (135°W to 45°W) responses. Each row corresponds to a different isobar used to index the QBO. The isobar is given on the right of each row [Colour figure can be viewed at wileyonlinelibrary.com]

3.2 | Modulation of planetary waves by the QBO

The QBO_{10} and QBO_{50} zonally averaged WAF response of Figure 1 is shown averaged over individual sectors in Figure 2, revealing distinct planetary wave responses over longitude for QBO_{10} and QBO_{50} ($QBO_{20-30-70}$ responses are given in Figure S5). The 3D WAF and its corresponding 3D divergence are calculated for all grid points for all 1,500 years of data. These fields are then split into four equally sized slices by longitude and averaged over longitude. This is accompanied by stereographic views of the vertical WAF at 850 and 50 hPa, in Figures 3 and 4, respectively.

The QBO uniformly suppresses equatorward propagation toward the QBO easterlies while allowing propagation toward the QBO westerlies (Figure 2). This is the strongest WAF response and is consistent regardless of QBO phase or longitudinal sector.

During QBO_{10}, there is enhanced upward WAF in the troposphere between 40°N and 60°N (Figure 1a) across all sectors but North America (Figure 2a–d). The climatological lower tropospheric vertical WAF is reinforced over the North Pacific, Siberia, and the North Atlantic (Figure 3a,b). The North Atlantic anomalous

WAF propagates toward the QBO westerlies (Figure 2a). The North Pacific anomalous WAF propagates upward and poleward (Figure 2c), with some of it passing into the stratosphere over the North Pacific (compare Figure 3a and 4a). In the stratosphere, the North Pacific anomalous upward WAF expands and intensifies between QBO_{10} and QBO_{20}, and then doubles in strength between QBO_{20} and QBO_{30} (Figure 4a–c).

During QBO_{50}, the tropospheric response is opposite of that during QBO_{10}, with both the climatological WAF reduced across all sectors and the climatological WAF convergence reduced at the tropopause (Figure 2e–g and 3d). In stark contrast to QBO_{10}, the anomalous upward WAF emanates from the tropopause around which there are WAF divergence anomalies. The North Atlantic anomalous WAF now propagates poleward and exhibits a "fountain-like" display as shown in White *et al.* (2015) (Figure 2e). At 50 hPa, we see an increase in the vertical WAF over the North Pacific (reinforcing the climatology, Figure 4f) that shifts easterly over Siberia as the lower stratospheric QBO phase becomes more easterly (Figure 4d,e). The anomalous stratospheric response leads to WAF convergence in the stratosphere over each sector except North America, with the largest responses observed over the North Pacific and Siberia (Figure 2e–g).

DJ 850 hPa WAFz (m²s⁻²)
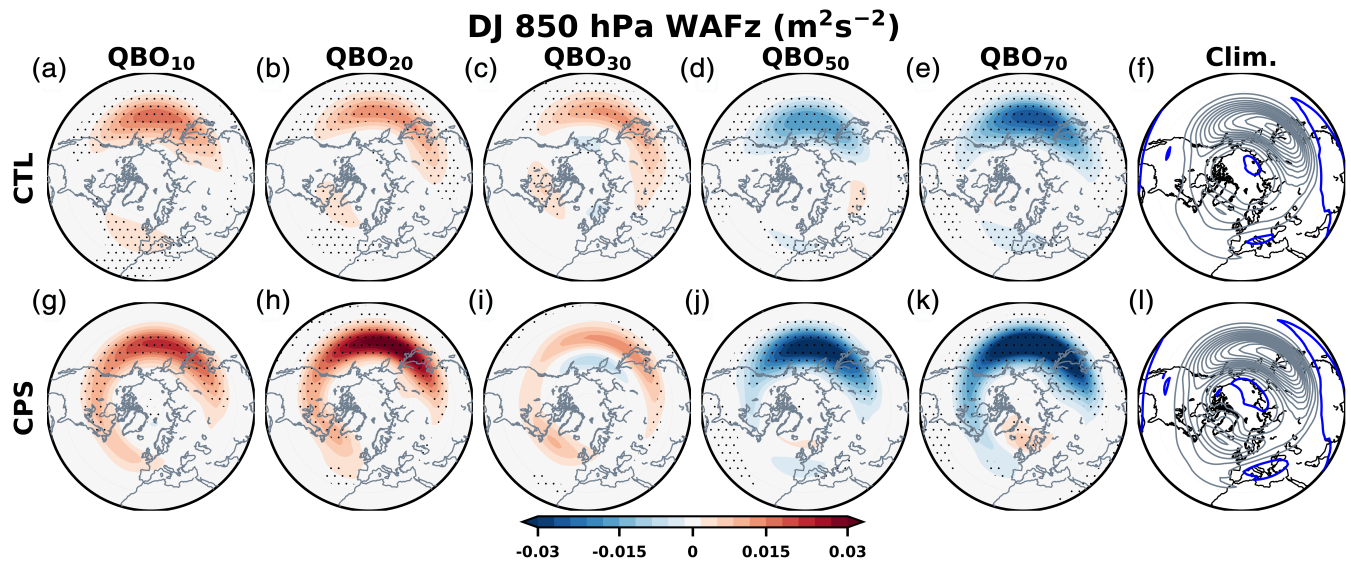
FIGURE 3 Polar stereographic views of the anomalous 850 hPa vertical WAF responses to the QBO in the CTL (top) and in CPS (bottom). The isobar used to index the QBO is found above the composites. Stippling is used to denote statistical significance. DJ climatologies in black contours are shown on the right with intervals of ±0.03 m²·s⁻² and the zero-contour shown in blue [Colour figure can be viewed at wileyonlinelibrary.com]

DJ 50 hPa WAFz (m²s⁻²)
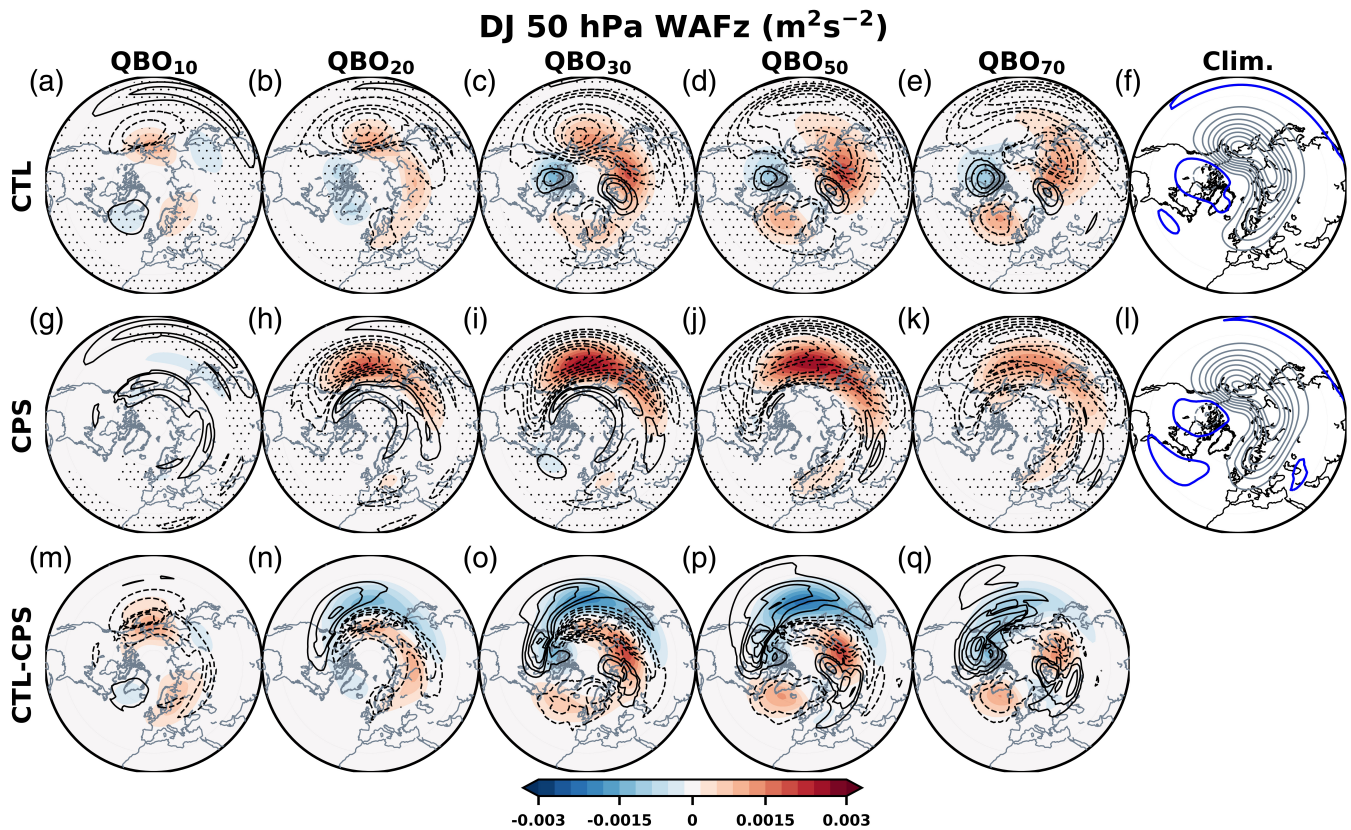
FIGURE 4 Polar stereographic views of the anomalous 50 hPa vertical WAF responses to the QBO in the CTL (top) and in CPS (middle). The isobar used to index the QBO is found above the composites. Stippling is used to denote statistical significance. Anomalous WAF divergence is overlaid with contour intervals of 0.0026 m·s⁻¹·day⁻¹ with the zero-contour omitted. Only the statistically significant responses are shown for the WAF divergence. DJ climatologies in black contours are shown on the right with intervals of ± 0.003 m²·s⁻². The difference between the CTL and CPS anomalies is shown in the bottom row [Colour figure can be viewed at wileyonlinelibrary.com]

In the North Atlantic, the QBO leads to increases in the upward WAF during QBO_{50-70} (Figure 4d,e) while the anomalous WAF is downward during QBO_{10-20} (Figure 4a,b). In climatology, the vertical WAF is nearly zero in the North Atlantic just south of Greenland (Figure 4f), suggesting upward propagating planetary waves are generated during QBO_{50-70} and downward propagating waves during QBO_{10}.

To better isolate the role of the QBO in generating the WAF responses, we examine the CPS experiment when the polar stratospheric variability is suppressed. In the lower troposphere, the main difference between CPS and CTL is that the CPS anomalies are larger in magnitude (Figure 3, bottom row). This suggests that the polar stratospheric response to QBO in the CTL reduces the direct forcing from QBO.

In the stratosphere, the anomalous upward WAF at 50 hPa in the North Pacific vanishes during QBO_{10}, but is present in QBO_{20-30} (Figure 4g–i). The easterly shift of this response from the North Pacific to Siberia as the QBO phase in the lower stratosphere becomes more easterly is less pronounced relative to CTL (compare Figure 4, top and middle). In fact, the dominant response in CPS is anomalous upward WAF in the North Pacific and corresponding WAF convergence there, occurring during $QBO_{20-30-50-70}$. Of all sectors, the North Pacific responses are most similar between CPS and CTL. For instance, note how similar the WAF divergence and (convergence) is between CTL and CPS during QBO_{10} (QBO_{70}) (Figure 4a,g,e,k): this response arises from the QBO, not polar stratospheric variability. This is interesting as it suggests that the QBO promotes the WAF response in the North Pacific with a secondary role for polar stratospheric variability there. This North Pacific WAF is part of the "direct effect" of the QBO on the extratropical atmosphere.

On the contrary, vertical WAF anomalies over North America, the North Atlantic, and Siberia vanish in CPS. This suggests that WAF responses in these sectors are mutually dependent on the QBO and polar stratospheric variability. This is generally true regardless of QBO phase. Polar stratospheric variability can be defined as the difference between the CTL and CPS responses to the QBO (Figure 4, bottom row). During QBO_{50} for instance, it accounts for anomalous downward WAF over North America, upward anomalies over the North Atlantic, and upward anomalies over Siberia (Figure 4p).

CPS promotes more WAF convergence over the North Pacific than in the CTL during $QBO_{20-30-50}$. The 2.5-hr relaxation timescale in CPS should preclude any planetary wave breaking in the polar stratosphere. With the anomalous waves not allowed to break within polar latitudes, wave breaking is enhanced in the extratropics, mainly over the North Pacific (compare Figure 4, top and middle).

The first inference we draw from this is that QBO initiates the lower stratospheric Holton–Tan effect through the North Pacific. Since the polar stratosphere cannot accept inbound waves, wave breaking is more vigorous in the mid-latitude stratosphere. Since the polar stratosphere cannot be disturbed, no downstream WAF changes may take place over North America, the North Atlantic, and Siberia. The "indirect effect," which takes place once the QBO modulates the polar stratosphere, is shut off in CPS. We will diagnose the spatiotemporal evolution of QBO-polar stratosphere coupling in sections 3d and 3e.

A final point is that the QBO-MMC appears to have some zonal asymmetries. During QBO_{50} and QBO_{70}, the residual circulation defining the QBO-MMC should move poleward from the QBO around 50 hPa. In the zonal mean, this poleward motion is consistent with convergence of the Eliassen–Palm flux (Figure 1d; fig. 3 of Hu and Tung, 2002; figs. 6 and 7 of White *et al.*, 2015). The 3D generalization of this field shows that the WAF convergence is primarily found over the North Pacific in CTL and CPS (Figure 4d,e,j,k) suggesting that the QBO-MMC is more localized to the North Pacific.

3.3 | Tropospheric response: Competition between the direct and indirect QBO effect

Since CPS suppresses the polar stratospheric response to the QBO, it presents an opportunity to assess the direct influence of the QBO on the extratropical zonal circulation. In Figure 5, the 200 hPa zonal wind response to the QBO is compared in CTL versus CPS. The CPS 200 hPa zonal wind anomalies (Figure 5f–j) are stronger and more zonally symmetric about the mid-latitudes than those in the CTL (Figure 5a–e), another indication that the QBO and polar stratospheric variability compete to alter extratropical flow.

Consistent with Figure 1, $QBO_{10-20-30}$ feature equatorward shifting jets (Figure 5a–c) while QBO_{50-70} feature poleward shifting jets (Figure 5d,e). Given the near superposition of the subtropical and eddy-driven jets in the North Pacific, the zonal wind response is consistent with an enhancement (weakening) of the jet during QBOW (QBOE). In the North Atlantic, the QBO prompts opposing responses with the distinct subtropical and eddy-driven jets. Regardless of sector, the CPS anomalies are stronger.

To investigate the apparent competition between the direct effect of the QBO and the polar stratospheric response to it in the troposphere, in Figure 6 we compare the CTL and CPS temperature (shading) and zonal wind (contours) responses in the North Pacific (135°E to 135°W), where the anomalies are largest (see

DJ 200 hPa U-wind (m/s)
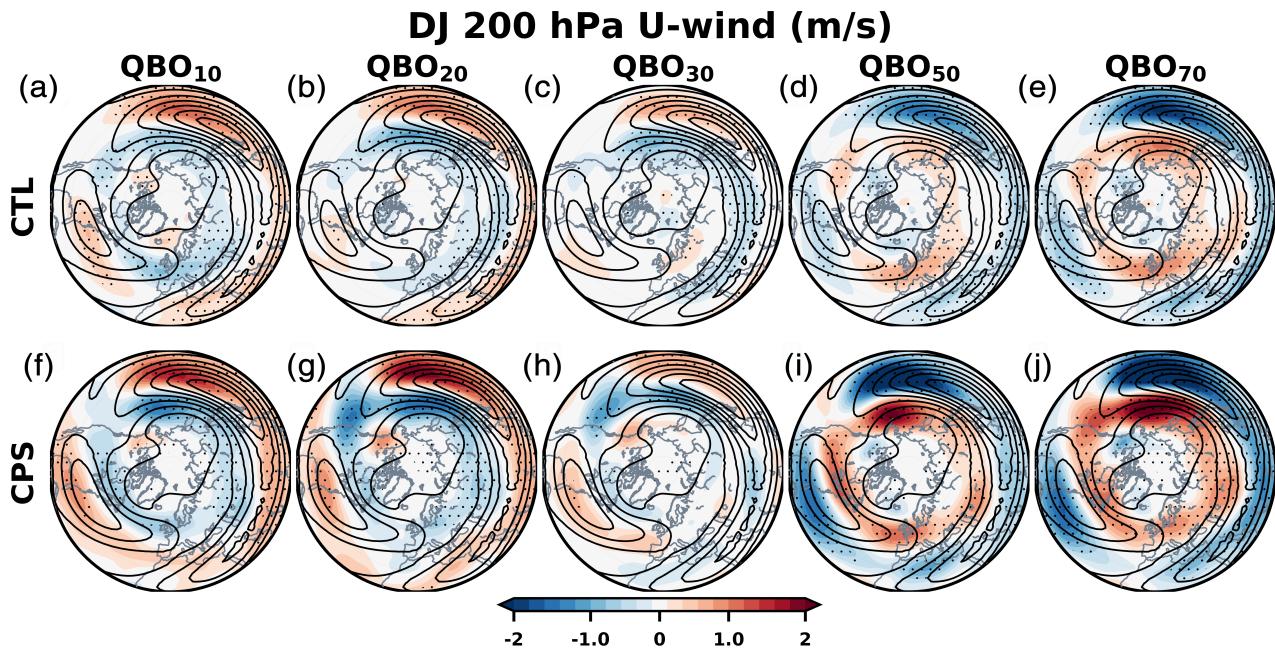
FIGURE 5 Polar stereographic views of the anomalous 200 hPa zonal wind responses to the QBO in the CTL (top) and in CPS (bottom). Wind anomalies are shaded, and stippling is used to denote statistical significance. The isobar used to index the QBO is found above the top panels. The DJ climatological wind is superimposed in black contours with contour levels of 10, 20, 30, 40, 50, 60, and 70 m·s^{-1} with no zero contour line [Colour figure can be viewed at wileyonlinelibrary.com]

Figure 5). The QBO has been shown to have a particularly strong impact in this sector (Garfinkel and Hartmann, 2011b).

Tropical heating and extratropical cooling manifest near the tropopause during QBO$_{10}$ in CTL and CPS (Figure 6a,f) in response to the QBO-MMC. As the upper tropospheric zonal wind field adjusts to the temperature anomalies, changes in the eddy momentum flux take place in the upper troposphere (see Figure 7 of both Garfinkel and Hartmann, 2011a; 2011b). These changes in the eddy momentum flux are compensated for by residual circulations in the troposphere wherein Coriolis accelerations in the aloft branch oppose the zonal wind anomalies created by the heating and cooling (Haigh *et al.*, 2005; Simpson *et al.*, 2009; Simpson *et al.*, 2012). Importantly, the descending (ascending) branch of the anomalous meridional circulation in the troposphere leads to adiabatic warming (cooling) of the mid and lower troposphere. This supports zonal wind anomalies developing deeper in the troposphere, thereby communicating the initial stratospheric temperature perturbations driven by the QBO-MMC into tropospheric zonal wind forcing.

During QBO$_{50}$ in the CTL (Figure 6d), the signal is reversed, with cold anomalies in the tropics, warming in the extratropics in response to the QBO-MMC, and polar warming consistent with the Holton–Tan effect. The heating and cooling centers as well as the response in zonal wind maintain thermal wind balance of the jet.

For CPS, two tropospheric secondary circulations oppose the dipole of zonal wind anomalies (Figure 6i), consistent with heating (cooling) at 500 hPa and 40°N (20°N and 65°N). This dipole of temperature anomalies supports the extension of westerlies and easterlies deeper into the troposphere.

We subtract the CPS anomalies from the CTL anomalies to highlight how the response of the polar stratosphere to the QBO competes with the direct tropospheric effect of the QBO (Figure 6, bottom row). As the polar stratosphere warms under QBO$_{30-70}$ (Figure 6m–o), the jet shifts equatorward in response to the polar warming, opposite to the poleward shift associated with the QBO-MMC effect observed in CPS (Figure 6h–j). In the troposphere, warm temperature anomalies are found in high latitudes (Figure 6n), as expected from downward propagation of the stratospheric warming through stratosphere–troposphere coupling mechanisms. This is opposite to the tropospheric temperature response in CPS (Figure 6i), which exhibits a cooling of high latitudes and a warming of mid latitudes consistent with reinforced westerlies and a positive Northern Annular Mode type of circulation anomaly (Thompson and Wallace, 1998). These two competing effects explain the moderate seasonal mean tropospheric cooling in the high latitudes during QBO$_{50}$ (Figure 6d). With QBO$_{10}$, since the polar stratosphere does not respond as strongly to the QBO, CTL and CPS are much more consistent (Figure 6a,f).

DJ Pacific Temp (K) and U-wind (m/s)
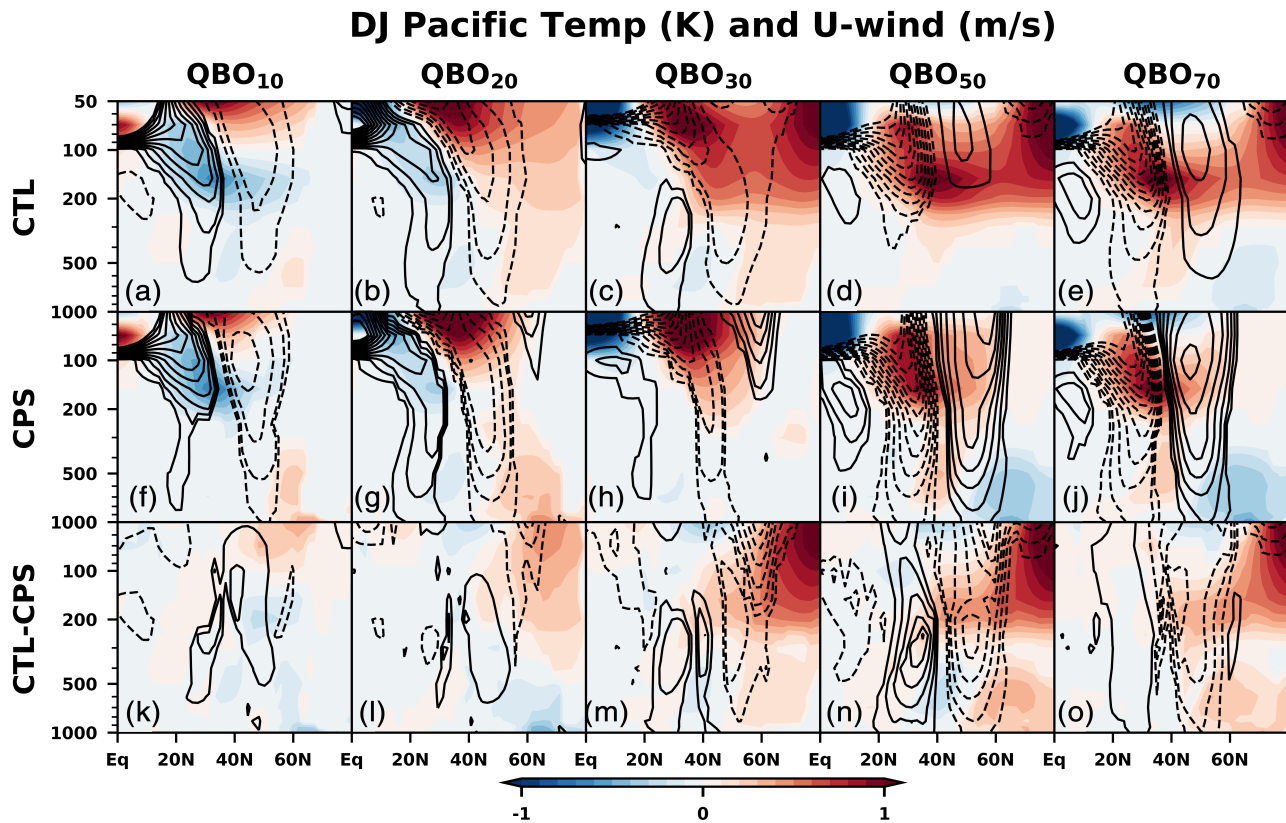
FIGURE 6 Pacific sector (135°E to 135°W) zonal mean zonal wind (black contours, 0.25 m·s⁻¹ interval) and temperature responses (shading) to the QBO. The first row features the CTL response, middle is for CPS, and the bottom is difference between CTL and CPS responses. The isobar used to index the QBO is the found above each column. Stippling is used to denote statistical significance [Colour figure can be viewed at wileyonlinelibrary.com]

In summary, we find that the tropospheric zonal wind and temperature anomalies directly driven by QBOE are moderated by the indirect effect of a warmer polar stratosphere during QBOE. Although this QBO–polar stratosphere competition is consistent among all sectors in the stratosphere, the stratosphere–troposphere coupling and tropospheric response is most pronounced in the North Pacific relative to North America, the North Atlantic, and Siberia (respectively, Figures S6–S8). This enhanced tropospheric response in the North Pacific may be due to the large climatological tropospheric planetary wave flux in this sector, which is thought to facilitate enhanced stratosphere–troposphere coupling (White *et al.*, 2019).

### 3.4 | Timing of the polar vortex response: Importance of the North Pacific

We look for which region of the polar stratosphere begins warming first during the Holton–Tan effect. Figure 7 shows the daily evolution of four slices of the 10 hPa polar cap (60°N–90°N) geopotential height anomalies: North Pacific (135°E to 135°W), North America (135°W to 45°W),

North Atlantic (45°W to 45°E), Siberia (45°E and 135°E). Only the prescribed present-day SST/SIC simulation is used (300 years total). We continue to index based on the December–January QBO phase only. The increases (QBOE) and decreases (QBOW) in height are consistent with the Holton–Tan effect, and the largest-magnitude responses occur over North America and the North Atlantic. Note the slant in geopotential height responses from the top left of Figure 7 toward the bottom right. The QBO affects when the polar cap warms: earlier during QBOE and later during QBOW with the North Pacific and North America responses leading the other sectors.

3.5 | Stratospheric wave response

In Figure 8, the 50 hPa geopotential height anomalies and 510 K potential vorticity (PV) anomalies reveal that the position of the polar cyclonic flow changes for each QBO phase. Heights decrease over North America during QBO$_{10}$ (Figure 8a) while they decrease over Eurasia as the QBO phase becomes more easterly (Figure 8c). As in section 3d, we see that the increases in height are largest

ONDJ 10 hPa Polar Cap GEOP (m)
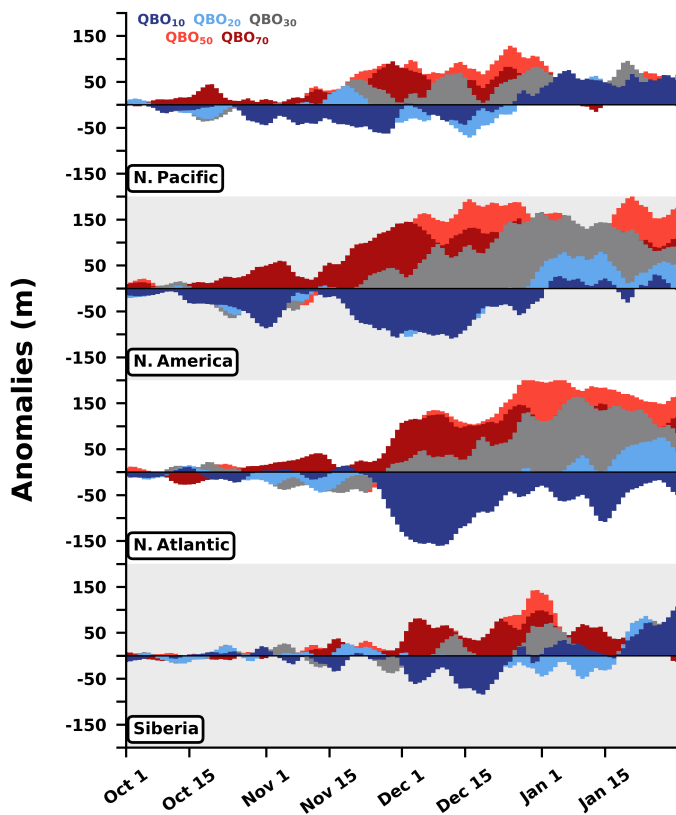
FIGURE 7 October to January (ONDJ) daily 10 hPa geopotential height anomalies (m) over the polar cap (60°N–90°N) and split amongst the four equally sized sectors: North Pacific (135°E to 135°W), North America (135°W to 45°W), North Atlantic (45°W to 45°E), and Siberia (45°E to 135°E). The five different colors are used to identify the isobar used to index the QBO. The QBO is indexed using only December and January. Daily anomalies from October and November are included for the analysis as well [Colour figure can be viewed at wileyonlinelibrary.com]

over North America and over the North Atlantic during QBO$_{30-50-70}$ (Figure 8c–e).

The position of the anomalous polar trough and polar warming, which vary by QBO phase, coincide with distinct potential vorticity gradients, each supporting different planetary wave responses. The 50 hPa three-dimensional wave activity flux anomalies reveal that the anomalous wave trains propagate along positive PV gradients. During QBO$_{30}$, the anomalous wave propagates east towards Eurasia away from the North Atlantic (Figure 8m) along the weak but positive anomalous PV gradient (Figure 8h). This is opposite of the QBO$_{10}$ response in which the wave propagates west toward the North Atlantic from Eurasia (Figure 8k). The following features are ubiquitous among all QBO phases: there is (a) propagation of the anomalous wave toward the anomalous polar trough, and (b) prominent WAF convergence in the North Pacific.

Figure 4 and now Figure 8 have both shown concurrent increases in the upward flux over the North Atlantic and Siberia during QBO$_{50-70}$. We speculate that this is associated with the position of the anomalous polar cyclonic flow, which is superimposed directly between these two anomalous upward WAF responses. This suggests that the spatiotemporal evolution of the polar cyclonic flow given a background QBO state (see section 3d) is important

because it preconditions the stratosphere to support planetary wave propagation. O'Neill and Pope (1988), for instance, find that interaction between polar stratospheric anticyclones and cyclonic flow promotes subsequent vacillations in the polar stratospheric wind. Moreover, the "wave forcing" they investigate is quite zonally asymmetric (as we are interested in), originating over the ocean basins in different examples. In our results, recall that both the North Atlantic and Siberia upward fluxes vanished in the absence of polar stratospheric variability (Figure 4). This all suggests that the spatiotemporal evolution of the polar stratospheric flow, following forcing by the QBO, promotes WAF over North America, the North Atlantic, and Siberia. We pose the following question: does the anomalous WAF over the North Pacific precede the change in polar stratospheric flow, which ultimately drives the upward WAF over the North Atlantic? We answer this using the transient simulations in which we impose QBOE and QBOW profiles.

The control transient simulation features no QBO. We branch from November 1 of the control and turn on the QBO. Note that the QBO begins descending once the nudging is activated, and it takes about a month for the QBO-MMC to develop in the extratropics (not shown). The QBO is imposed so that it progresses toward the desired QBO profile by mid-December. The easterly QBO

CTL 50 hPa polar stratospheric response
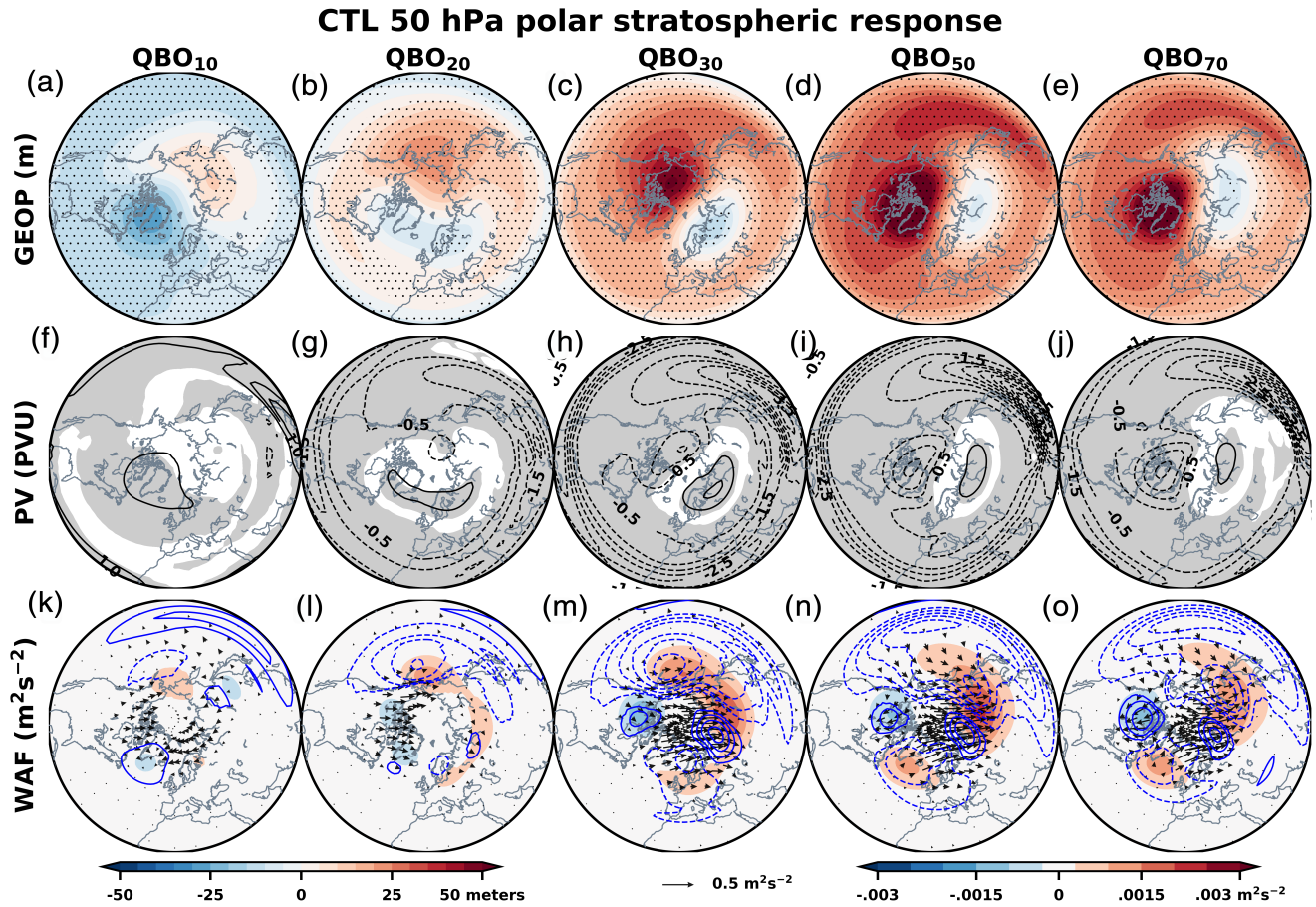
FIGURE 8   Polar stereographic views of the DJ 50 hPa responses to the QBO. Each column corresponds to a different isobar used to index the QBO. This isobar is indicated above each column of plots. Row one shows the geopotential height responses, row two the 510 Kelvin PV responses, and row three the 3D WAF responses. Geopotential height anomalies are shaded, and stippling denotes statistical significance. PV anomalies are shown in contours with an interval of ± 0.5 PVU, and gray shading denotes statistical significance. For the 3D WAF, the vertical component is shaded, the meridional and zonal components are shown as vectors, and WAF divergence is shown in blue contours with intervals of $\pm 0.0026 \, \mathrm{m \cdot s^{-1} \cdot day^{-1}}$, excluding the zero contour. Only statistically significant responses are shown for the bottom row [Colour figure can be viewed at wileyonlinelibrary.com]

simulation exhibits the QBO_{50} profile, and the westerly QBO simulation exhibits the QBO_{10} profile.

Figure 9 shows the 50 hPa WAF anomalies in the transient simulations with the horizontal components shown as vectors, the vertical component in shading, and the divergence of the WAF in blue contours. Anomalies are defined as the QBO_{50} minus QBO_{10} responses. In the first 50 days, enhanced upward and poleward WAF is observed in the North Pacific and over Siberia resulting in WAF convergence in those regions (Figure 9a,e). This is consistent with erosion of the 510 K PV gradient over East Asia above the subtropical jet region (Figure 9b,f). Note the negative PV anomalies circling the lower extratropics. This arises from the divergent poleward flow of the QBO-MMC during QBO_{50}, which should be contrasted with the "pinching" of the PV field by the convergent equatorward flow of the QBO-MMC during QBOW (fig. 1 of Hitchman and Huesmann, 2009). Vorticity and geopotential are

related by a Laplacian operator, hence the negative PV anomalies coincide with increases in geopotential height (Figure 9c,g). The height anomalies increase over Siberia and the North Pacific from days 11–30 to days 31–50 and then expand eastward. This follows the same spatiotemporal evolution of geopotential heights in the seasonal mean (Figure 7). This continues through days 51–92 as the height anomalies increase and encroach on the polar stratosphere (Figure 9k,o). Meanwhile in the upper troposphere, the jet shifts poleward once the QBO-MMC becomes established in the extratropics (Figure 9, right column). This mimics the seasonal mean U200 response (Figure 5d).

For the duration of the transient simulations, the North Pacific sector (defined as 135°E to 135°W) and the easternmost part of our Siberia sector (defined as 45°E to 135°E) dominate the mid-to-high latitude WAF response. Recalling the results of the previous section, we conclude that the Holton–Tan effect is primarily mediated

QBO$_{50}$-QBO$_{10}$ 50 hPa Response
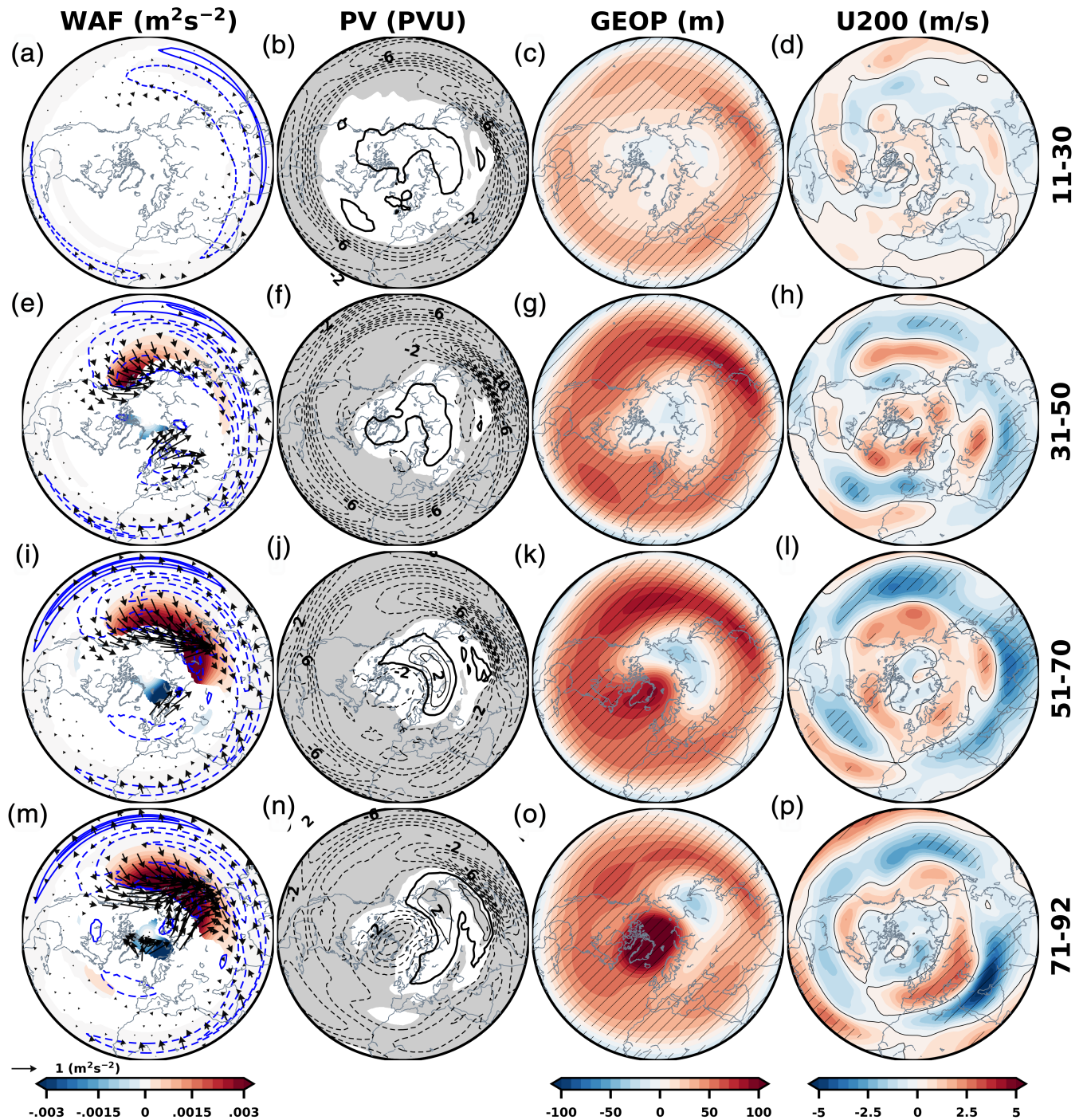
FIGURE 9 Polar stereographic views of the 50 hPa atmospheric response to turning on the QBO in the branched simulations. Anomalies are calculated as the difference between the QBO50 and QBO10 branched runs, which highlights the response to QBOE. Row one shows the response over days 11–30, row two: days 31–50, row three: days 51–70, and row four: days 71–92. From left to right, column one shows the 3D WAF response. The vertical component is shaded, the meridional and zonal components are shown as vectors, and WAF divergence is shown in contours with an interval of ±0.00864 m·s^{-1}·day^{-1}, excluding the zero contour. Only statistically significant responses are shown. Column two shows the 510 Kelvin PV response. The contour interval is ±1 PVU, and gray shading denotes statistical significance. Column three shows the geopotential height response in shading, and hatching denotes statistical significance. Column four shows the 200 hPa zonal wind response with hatching used to denote statistical significance [Colour figure can be viewed at wileyonlinelibrary.com]

through the North Pacific high latitudes in the lower stratosphere.

The strong erosion of the PV gradient over the Siberian sector explains why. The PV field weakens in the extratropics around 135°E as soon as the branching begins and for the entirety of the runs (Figure 9, second column). In the upper troposphere, wave breaking typically occurs east of the jet core near jet exit regions because the waning PV gradient provides diminishing support to Rossby wave propagation (Abatzoglou and Magnusdottir, 2006). Consistent with this, WAF convergence occurs throughout the North Pacific downstream of where the PV gradient has been weakened (compare Figure 9, first and second columns). This then initiates the circumpolar warming. In response to the question posed in this section, the anomalous WAF response over the North Pacific leads to changes in the polar stratospheric flow.

At no point in the transient simulations is there anomalous upward WAF in the North Atlantic reminiscent of the signal discussed in section 3b (compare first column of Figures 9 and 4d). This response exists but is not statistically significant. Because we suspect that the North Atlantic upward WAF is dependent on the polar stratospheric flow, we composite on the December through January daily vertical WAF in this region: 60°W to the Prime Meridian and 45°N to 75°N (box shown in Figure 10a). This is done using daily data from the 300-year simulation set forced with prescribed present-day climatological SST and SIC, the QBO_{10} transient run, and the QBO_{50} transient run. Results are consistent for all three simulations, so we only show the first.

The days with the maximum and minimum vertical WAF in the North Atlantic box are selected for each year. These are referred to as "upward" and "downward" events, respectively. Both upward and downward WAF days are distributed evenly throughout the December and January period (not shown). Figure 10 shows the 510 K (~50 hPa) isentropic potential vorticity anomalies and full field (anomaly + climatology) corresponding to the two types of events.

The polar vortex exhibits very different configurations for each event type. For the upward case, the polar vortex shifts toward Eurasia (Figure 10c), while for the downward case, it shifts towards North America (Figure 10f). In reanalysis, Zhang *et al.* (2019) find a shift of the polar vortex toward Eurasia during QBOE and a shift towards North America during QBOW. Our results corroborate this. During QBO_{10} (a QBOW background state), negative vertical WAF anomalies are found in the North Atlantic (Figures 4a and 8k). Negative vertical WAF anomalies in the North Atlantic are associated with a shift of the polar vortex toward North America (Figure 10f). A shift of the polar vortex toward North America is observed

N. Atlantic 50 hPa WAFz composites
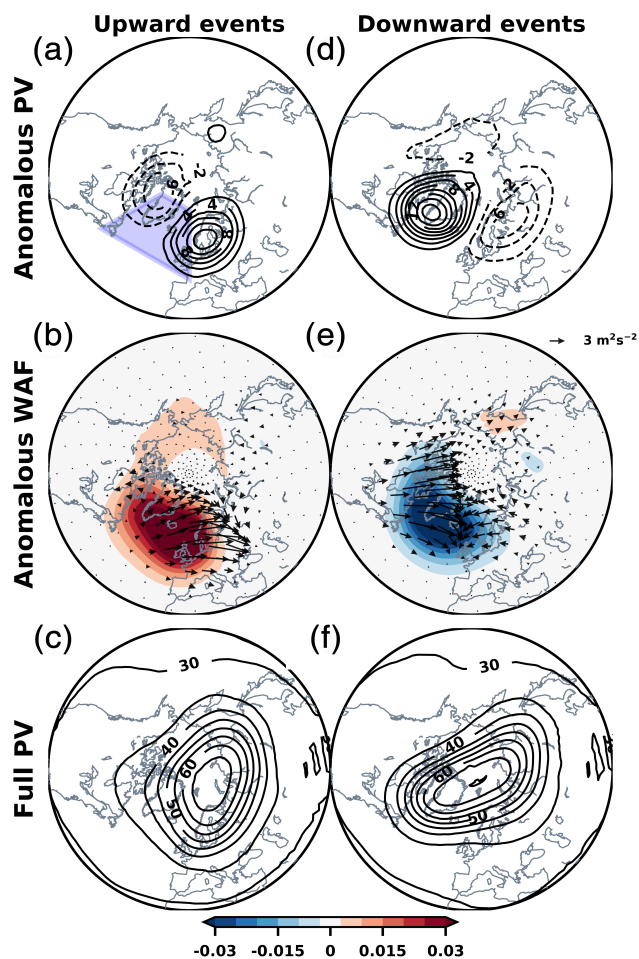
FIGURE 10 510 K potential vorticity (PV) and 50 hPa 3D WAF composites of "upward" and "downward" events in the North Atlantic stratosphere. Refer to text for details on how these plots are created. From left to right, column one shows responses for upward events, and column two shows that for downward events. Row one shows the anomalous PV response, row two the anomalous WAF response, and row three the full PV field corresponding to these events. This is denoted on the left of column one. Composite (a) shows the domain over which the vertical WAF is averaged to create the indices for upward and downward events: 60°W to the prime Meridian and 45°N to 75°N [Colour figure can be viewed at wileyonlinelibrary.com]

to occur during QBOW (Zhang *et al.*, 2019). The opposite applies during QBOE. The position of the polar vortex, which shows modulation by the QBO on reanalysis, appears to be associated with distinct WAF responses. The anomalous horizontal wave response (Figure 10b,e) always moves up the PV gradient toward the highest PV anomaly (Figure 10a,d), which is the expected wave behavior (McIntyre and Palmer, 1985; McIntyre, 1992). The anomalous PV/WAF responses associated with upward (downward) events mimic the seasonal mean PV/WAF responses for QBO_{50} (QBO_{10}) (Figure 8, column one, four).

ERA5 50 hPa polar stratospheric response
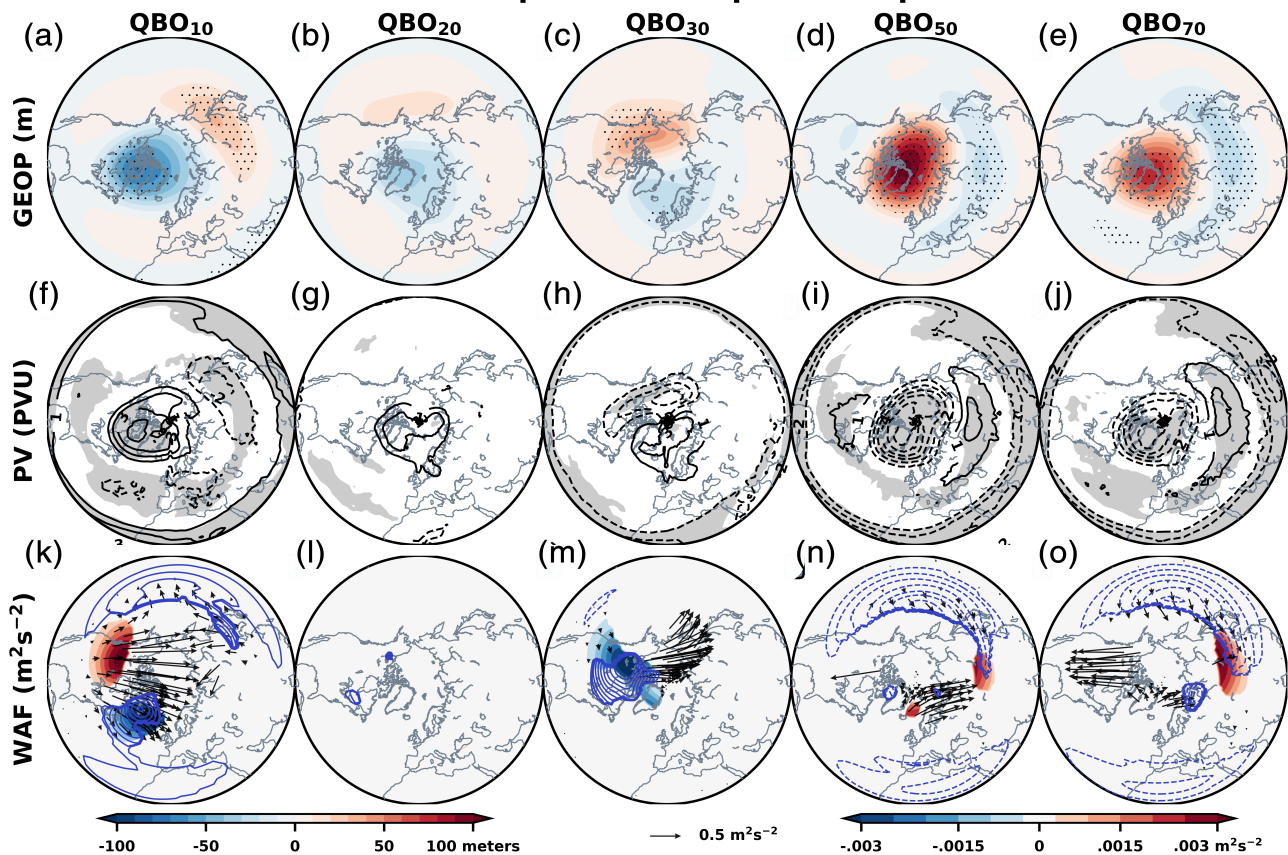
FIGURE 11 As in Figure 8, but for ERA5. The geopotential height anomaly colorscale ranges from 100 to −100 m now to account for the stronger responses in ERA5 [Colour figure can be viewed at wileyonlinelibrary.com]

In the transient runs, the missing ingredient for a robust upward WAF response in the North Atlantic appears to be the shift of the polar vortex toward Eurasia in the mean response (compare Figure 9n with Figure 10a). The degradation of the PV field over Greenland between days 71 and 92 mimics the anomalous PV response associated with upward WAF in the North Atlantic (Figure 10a). However, there is no concurrent increase in the PV field over Eurasia during the transient simulations, which would indicate a shift of the polar vortex. This again indicates that the polar cyclonic flow is essential for upward WAF in the North Atlantic. Reasons for the absence of the polar vortex shift towards Eurasia in the transient runs, when compared with the 1,500-year run, may reside in the different QBO profile imposed in each experiment. A single and specific QBO profile is imposed in each ensemble member of the transient runs, while the seasonal mean anomalies result from an average of distinct QBO profiles (due to the "walking down" prescription of the QBO). Further work is needed to understand this question.

There is mounting evidence that the QBO teleconnection with the high-latitude stratosphere is mediated through the combined North Pacific and Siberia sectors.

Other studies show that the extratropical circulation north of the Maritime Continent is responsive to the QBO (Chen and Li, 2007; Garfinkel and Hartmann, 2011b; Wang *et al.*, 2018) and this region exhibits strong planetary wave breaking during boreal winter (Hitchman and Huesmann, 2009). This is not too unexpected considering that this is a region of large baroclinicity, where the strongest boreal winter westerlies are found in climatology, consistent with the local land-sea contrast, orography (White *et al.*, 2017), and strong convection over the Maritime Continent.

3.6 | Reanalysis results

We now look to see if our findings from the model experiments are consistent with ERA5 reanalysis. In Figure 11, we show the 50 hPa geopotential height response, the 510 K PV response, and the 50 hPa wave activity flux response. This figure is the reanalysis equivalent of Figure 8, with the only difference being that the geopotential height color scale ranges from −100 to 100 m rather from −50 to 50 m. Using data from 1979–2019, we

end up with just ~13 December–January periods that are used to make each composite.

The 50 hPa geopotential height responses (Figure 11, first row) are generally consistent between ERA5 and SC-WACCM4, with anomalies that are roughly 3–4 times stronger in ERA5. This may be explained in part by the lack of dynamic chemistry in our specified chemistry simulations (Silverman *et al.*, 2018), but also by the influence of internal variability that affects short observational records. The PV response shows that the position of the polar cyclonic flow varies with the background QBO state, similar to SC-WACCM4. The polar cyclone is reinforced closer to North America during QBO_{10} (Figure 11a,f), but shifts toward Eurasia as the QBO phase in the lower stratosphere becomes more easterly (e.g., Figure 11d,i). Similar to the geopotential height response, the PV response is far stronger in ERA5 relative to SC-WACCM4. QBO_{50} shows a 6 PVU degradation of the polar flow over North America versus a 2 PVU degradation for SC-WACCM4 (Figure 11i vs. 8i). Ridging of the polar cap is more zonally symmetric about the pole in ERA5 during QBO_{50-70} compared with SC-WACCM4 (Figure 11d,e).

The WAF results (Figure 11, third row) agree well with SC-WACCM4. There is enhanced upward WAF over part of the North Pacific (but also North America) during QBO_{10} (Figure 11k), which shifts easterly toward Siberia during QBO_{50-70} (Figure 11n,o). A key finding is that the enhancement of upward (downward) WAF in the North Atlantic during QBOE (QBOW) exists in ERA5. Using the period 1979–2017, these vertical WAF results are reproduced in National Centers for Environmental Prediction (NCEP)–National Center for Atmospheric Research (NCAR) reanalysis dataset (Kalnay *et al.*, 1996) (not shown). Given that plenty of internal variability is available to convolute these results and that each composite is made from only 13 seasons in ERA5 as opposed to 500 seasons in SC-WACCM4, these reanalysis findings bolster our argument that QBO has a dominant impact in the North Atlantic. Furthermore, across all sectors, both the ERA5 and NCEP WAF anomalies are roughly two to three times larger than the response in the 1,500-year CTL. A final key finding is that WAF divergence responses over the North Pacific during all QBO phases are consistent with SC-WACCM4, again indicating an important role for this longitudinal sector in the teleconnection between the QBO and polar stratosphere (Figure 11l–o).

4 | CONCLUSIONS AND DISCUSSION

Coming back to the key questions identified in the introduction, here is a summary of our findings:

4.1 | How does the extratropical response evolve with the QBO cycle?

With the large sample size in our simulations, we identify that the extratropical response to the QBO is phased with the QBO cycle. Each QBO phase has an impact on both the troposphere and the polar stratosphere, with remarkable linearity in the signal from QBO_{10} to QBO_{70}. To capture the full range of the QBO effect, a cyclic approach (e.g., Huesmann and Hitchman, 2001 or Gray *et al.*, 2018) must be applied, because defining the QBO at one level only captures a fraction of the QBO influence in the extratropics.

4.2 | How does the QBO effect vary over longitude?

We find robust evidence for the Holton–Tan effect during December and January in SC-WACCM4 with 1,500 years of data. Our results reveal that the atmospheric response to the QBO is asymmetric in longitude. We consistently find evidence that the QBO has the greatest impact on the extratropical circulation north of the Maritime Continent and northeast toward Alaska (our North Pacific and Siberian sectors). As suggested by the CPS simulation, which suppresses the feedback from the polar stratosphere, the upward wave activity flux anomalies in the North Pacific represent a direct response to the QBO, while wave activity flux anomalies in the North Atlantic sector are a consequence of the polar stratospheric response. The initial response of the polar cap is over the North Pacific. It follows from erosion of the PV gradient over Siberia, which prompts wave activity flux convergence downstream over the North Pacific. The associated increase in geopotential height then moves east downstream. We find this both in the seasonal mean analyses and when analyzing the transient simulations, evidence that the lower stratospheric branch of the Holton–Tan effect proceeds through the North Pacific high latitudes.

The spatiotemporal evolution of the polar stratosphere then becomes important. A shift of the polar vortex toward Eurasia is consistent with an upward stationary wave activity flux in the North Atlantic. Conversely, a shift of the polar vortex toward North America is associated with downward wave propagation in the North Atlantic. In this regard, lower stratospheric wave activity flux anomalies in the North Atlantic do not drive the polar vortex response, although they play a role in amplifying the response. Our SC-WACCM4 results generally suggest that the polar vortex shifts towards Eurasia during easterly QBO and toward North America during westerly QBO. This is consistent with ERA5 and corroborates Zhang *et al.* (2019).

Our CPS simulation also reveals that there is a competing effect between the midlatitude jet response to the QBO (poleward shift) and feedback of the polar stratosphere (equatorward shift), which is most pronounced over the North Pacific. This has implications for seasonal forecasting because it implies that the influence of the QBO on the troposphere may vary from 1 year to another depending on the state of the polar stratosphere and how it evolves in response to the QBO. This result also has implications for model evaluations of the QBO because if models exhibit different sensitivity of the polar stratosphere to the QBO, these differences will likely be reflected in the model tropospheric response to the QBO. Recently, Richter *et al.* (2020) has shown that many CMIP6 models, which spontaneously generate the QBO, underestimate the QBO's amplitude in the lower stratosphere. This, coupled with the variation in how the models represent the Holton–Tan effect (Rao *et al.*, 2020), implies that there will be spread in the modeled tropospheric responses to the QBO.

4.3 | What is the impact of the QBO on the extratropical atmosphere versus that from polar stratospheric variability?

An interesting finding is that near the surface and in the lower troposphere, the climatological wave activity is actually enhanced under QBOW. However, the majority of waves break at the tropopause (only over the North Pacific), and there is little perturbation of the flow aloft in the polar stratosphere. Conversely, the perturbation of the polar vortex under QBOE is associated with wave activity flux convergence from planetary waves that originate in the upper troposphere. This SC-WACCM4 result supports the finding that increased planetary wave activity flux convergence in the polar stratosphere under QBOE is driven by the QBO-MMC and associated poleward shift of the tropospheric jet (White *et al.*, 2015). An interesting question to investigate going forward is what mechanism associated with the QBO may promote upward wave activity flux from the tropopause (e.g., Boljka and Birner, 2020).

We conjecture that the stronger QBO effect found over our Siberia and North Pacific sectors is due to specificities of those sectors, namely the sharp orography and land-sea contrast, which make it the sector with the strongest subtropical jet and stationary wave activity in the northern hemisphere (White *et al.*, 2017). We also note that the QBO is not exactly symmetrical (not shown here, Tegtmeier *et al.*, 2020), and the QBO winds have the strongest amplitude over the Maritime Continent. Perhaps it is the variability of the QBO itself that controls its meridional extent

(Haynes, 1998) and proximately the meridional extent of the QBO-MMC.

While our approach is unique from many others in that we focus on the zonally *asymmetric* rather than zonally averaged relationship between the QBO and polar stratosphere, our study is limited because we do not highlight the QBO's relationship with the upper polar stratosphere. It is likely that the three-dimensional structure of the polar stratosphere is important in controlling the upward wave activity fluxes. The QBO's teleconnection through the upper stratosphere, which is known to exist (Gray *et al.*, 2003; Ruzmaikin *et al.*, 2005; Garfinkel *et al.*, 2012; Lu *et al.*, 2014; Rao *et al.*, 2020; Lu *et al.*, 2020), may precondition the vortex to support these wave activity fluxes. Evaluating zonal asymmetry in the upper stratospheric teleconnection between the QBO and polar stratosphere (from 5–20 hPa) is a topic for future work.

ORCID
Dillon Elsbury https://orcid.org/0000-0002-3730-9226
Yannick Peings https://orcid.org/0000-0001-6852-7333
Gudrun Magnusdottir https://orcid.org/0000-0001-6079-5886

REFERENCES
Abatzoglou, J.T. and Magnusdottir, G. (2006) Planetary wave breaking and nonlinear reflection: seasonal cycle and interannual variability. *Journal of Climate*, 19, 6139–6152. https://doi.org/10.1175/JCLI3968.1.

Andrews, M.B., Knight, J.R., Scaife, A.A., Lu, Y., Wu, T., Gray, L.J. and Schenzinger, V. (2019) Observed and simulated teleconnections between the stratospheric quasi-biennial oscillation and northern hemisphere winter atmospheric circulation. *Journal of Geophysical Research: Atmospheres*, 124, 1219–1232. https://doi.org/10.1029/2018JD029368.

Anstey, J.A. and Shepherd, T.G. (2014) High-latitude influence of the quasi-biennial oscillation. *Quarterly Journal of the Royal Meteorological Society*, 140, 1–21. https://doi.org/10.1002/qj.2132.

Boljka, L. and Birner, T. (2020) Tropopause-level planetary wave source and its role in two-way troposphere–stratosphere coupling. *Weather and Climate Dynamics*, 1(2), 555–575. https://doi.org/10.5194/wcd-1-555-2020.

Bushell, A.C., Anstey, J.A., Butchart, N., Kawatani, Y., Osprey, S.M., Richter, J.H., Serva, F., Braesicke, P., Cagnazzo, C., Chen, C.-C., Chun, H.-Y., Garcia, R.R., Gray, L.J., Hamilton, K., Kerzenmacher, T., Kim, Y.-H., Lott, F., McLandress, C., Naoe, H., Scinocca, J., Smith, A.K., Stockdale, T.N., Versick, S., Watanabe, S., Yoshida, K. and Yukimoto, S. (2020) Evaluation of the quasi-biennial oscillation in global climate models for the SPARC QBO-initiative. *Quarterly Journal of the Royal Meteorological Society*, 1–31. https://doi.org/10.1002/qj.3765.

Butler, A.H., Sjoberg, J.P., Seidel, D.J. and Rosenlof, K.H. (2017) A sudden stratospheric warming compendium. *Earth System Science Data*, 9, 63–76. https://doi.org/10.5194/essd-9-63-2017.

Charlton, A.J. and Polvani, L.M. (2007) A new look at stratospheric sudden warmings. Part I: climatology and modeling benchmarks. *Journal of Climate*, 20, 449–469. https://doi.org/10.1175/JCLI3996.1.

Chen, W. and Li, T. (2007) Modulation of northern hemisphere wintertime stationary planetary wave activity: east Asian climate relationships by the quasi-biennial oscillation. *Journal of Geophysical Research*, 112, D20120. https://doi.org/10.1029/2007JD008611.

Collimore, C.C., Martin, D.W., Hitchman, M.H., Huesmann, A. and Waliser, D.E. (2003) On the relationship between the QBO and tropical deep convection. *Journal of Climate*, 16, 2552–2568. https://doi.org/10.1175/1520-0442(2003)016<2552:OTRBTQ>2.0.CO;2.

Coy, L., Wargan, K., Molod, A.M., McCarty, W.R. and Pawson, S. (2016) Structure and dynamics of the quasi-biennial oscillation in MERRA-2. *Journal of Climate*, 29, 5339–5354. https://doi.org/10.1175/JCLI-D-15-0809.1.

Dunkerton, T.J. and Baldwin, M.P. (1991) Quasi-biennial modulation of planetary-wave fluxes in the northern hemisphere winter. *Journal of the Atmospheric Sciences*, 48, 1043–1061. https://doi.org/10.1175/1520-0469(1991)048<1043:QBMOPW>2.0.CO;2.

Edmon, H.J., Hoskins, B.J. and McIntyre, M.E. (1980) Eliassen-palm cross sections for the troposphere. *Journal of the Atmospheric Sciences*, 37, 2600–2616. https://doi.org/10.1175/1520-0469(1980)037<2600:EPCSFT>2.0.CO;2.

Eichelberger, S.J. and Hartmann, D.L. (2007) Zonal jet structure and the leading mode of variability. *Journal of Climate*, 20, 5149–5163. https://doi.org/10.1175/JCLI4279.1.

Fletcher, C.G. and Kushner, P.J. (2011) The role of linear interference in the annular mode response to tropical SST forcing. *Journal of Climate*, 24, 778–794. https://doi.org/10.1175/2010JCLI3735.1.

Garfinkel, C.I. and Hartmann, D.L. (2010) The influence of the quasi-biennial oscillation on the North Pacific and El Niño teleconnections. *Journal of Geophysical Research*, 115, D20116. https://doi.org/10.1029/2010JD014181.

Garfinkel, C.I. and Hartmann, D.L. (2011a) The influence of the quasi-biennial oscillation on the troposphere in wintertime in a hierarchy of models. Part I: simplified dry GCMs. *Journal of the Atmospheric Sciences*, 68, 1273–1289. https://doi.org/10.1175/2011JAS3665.1.

Garfinkel, C.I. and Hartmann, D.L. (2011b) The influence of the quasi-biennial oscillation on the troposphere in wintertime in a hierarchy of models. Part II: perpetual winter WACCM runs. *Journal of the Atmospheric Sciences*, 68, 2026–2041. https://doi.org/10.1175/2011JAS3702.1.

Garfinkel, C.I., Shaw, T.A., Hartmann, D.L. and Waugh, D.W. (2012) Does the Holton–Tan mechanism explain how the quasi-biennial oscillation modulates the Arctic polar vortex? *Journal of the Atmospheric Sciences*, 69, 1713–1733. https://doi.org/10.1175/JAS-D-11-0209.1.

Garfinkel, C.I., White, I., Gerber, E.P., Jucker, M. and Erez, M. (2020) The building blocks of northern hemisphere wintertime stationary waves. *Journal of Climate*, 33, 5611–5633.

Gray, L.J., Anstey, J.A., Kawatani, Y., Lu, H., Osprey, S. and Schenzinger, V. (2018) Surface impacts of the quasi biennial oscillation. *Atmospheric Chemistry and Physics*, 18, 8227–8247. https://doi.org/10.5194/acp-18-8227-2018.

Gray, L.J., Drysdale, E.F., Lawrence, B.N. and Dunkerton, T.J. (2001b) Model studies of the interannual variability of the northern-hemisphere stratospheric winter circulation: the role of the quasi-biennial oscillation. *Quarterly Journal of the Royal Meteorological Society*, 127, 1413–1432. https://doi.org/10.1002/qj.49712757416.

Gray, L.J., Phipps, S.J., Dunkerton, T.J., Baldwin, M.P., Drysdale, E.F. and Allen, M.R. (2001a) The influence of the equatorial upper stratosphere on northern hemisphere stratospheric sudden warmings. *Quarterly Journal of the Royal Meteorological Society*, 127, 1985–2003. https://doi.org/10.1002/qj.49712757607.

Gray, L.J., Sparrow, S., Juckes, M., O'Neill, A. and Andrews, D.G. (2003) Flow regimes in the winter stratosphere of the northern hemisphere. *Quarterly Journal of the Royal Meteorological Society*, 129, 925–945. https://doi.org/10.1256/qj.02.82.

Haigh, J.D., Blackburn, R. and Day, R. (2005) The response of tropospheric circulation to perturbations in lower-stratospheric temperature. *Journal of Climate*, 18, 3672–3685. https://doi.org/10.1175/JCLI3472.1.

Haynes, P.H. (1998) The latitudinal structure of the quasi-biennial oscillation. *Quarterly Journal of the Royal Meteorological Society*, 124, 2645–2670. https://doi.org/10.1002/qj.49712455206.

Hersbach, H., Bell, B., Berrisford, P., Hirahara, S., Horányi, A., Muñoz-Sabater, J., Nicolas, J., Peubey, C., Radu, R., Schepers, D., Simmons, A., Soci, C., Abdalla, S., Abellan, X., Balsamo, G., Bechtold, P., Biavati, G., Bidlot, J., Bonavita, M., De Chiara, G., Dahlgren, P., Dee, D., Diamantakis, M., Dragani, R., Flemming, J., Forbes, R., Fuentes, M., Geer, A., Haimberger, L., Healy, S., Hogan, R.J., Hólm, E., Janisková, M., Keeley, S., Laloyaux, P., Lopez, P., Lupu, C., Radnoti, G., de Rosnay, P., Rozum, I., Vamborg, F., Villaume, S. and Thépaut, J.-N. (2020) The ERA5 global reanalysis. *Quarterly Journal of the Royal Meteorological Society*, 146, 1999–2049. https://doi.org/10.1002/qj.3803.

Hitchman, M.H. and Huesmann, A.S. (2009) Seasonal influence of the quasi-biennial oscillation on stratospheric jets and Rossby wave breaking. *Journal of the Atmospheric Sciences*, 66, 935–946. https://doi.org/10.1175/2008JAS2631.1.

Holton, J.R. and Tan, H.-C. (1980) The influence of the quasi-biennial oscillation on the global circulation at 50 mb. *Journal of the Atmospheric Sciences*, 37, 2200–2208. https://doi.org/10.1175/1520-0469(1980)037<2200:TIOTEQ>2.0.CO;2.

Holton, J.R. and Tan, H.-C. (1982) The quasi-biennial oscillation in the northern hemisphere lower stratosphere. *Journal of the Meteorological Society of Japan. Series II*, 60, 140–148. https://doi.org/10.2151/JMSJ1965.60.1_140.

Huesmann, A.S. and Hitchman, M.H. (2001) The stratospheric quasi-biennial oscillation in the NCEP reanalyses: climatological structures. *Journal of Geophysical Research: Atmospheres*, 106, 11859–11874. https://doi.org/10.1029/2001JD900031.

Kalnay, E., Kanamitsu, M., Kistler, R., Collins, W., Deaven, D., Gandin, L., Iredell, M., Saha, S., White, G., Woollen, J. and Zhu, Y. (1996) The NCEP/NCAR 40-year reanalysis project. *Bulletin of the American meteorological Society*, 77(3), 437–472.

Kinnersley, J.S. (1999) Seasonal asymmetry of the low-and middle-latitude QBO circulation anomaly. *Journal of the Atmospheric Sciences*, 56, 1140–1153. https://doi.org/10.1175/1520-0469(1999)056<1140:SAOTLA>2.0.CO;2.

Lorenz, D.J. and Hartmann, D.L. (2001) Eddy–zonal flow feedback in the southern hemisphere. *Journal of the Atmospheric Sciences*, 58, 3312–3327. https://doi.org/10.1175/1520-0469(2001)058<3312:EZFFIT>2.0.CO;2.

Lorenz, D.J. and Hartmann, D.L. (2003) Eddy–zonal flow feedback in the northern hemisphere winter. *Journal of Climate*, 16, 1212–1227. https://doi.org/10.1175/1520-0442(2003)16<1212:EFFITN>2.0.CO;2.

Lu, H., Baldwin, M.P., Gray, L.J. and Jarvis, M.J. (2008) Decadal-scale changes in the effect of the QBO on the northern stratospheric polar vortex. *Journal of Geophysical Research*, 113(D10). https://doi.org/10.1029/2007JD009647.

Lu, H., Bracegirdle, T.J., Phillips, T., Bushell, A. and Gray, L.J. (2014) Mechanisms for the Holton–Tan relationship and its decadal variation. *Journal of Geophysical Research: Atmospheres*, 119, 2811–2830. https://doi.org/10.1002/2013JD021352.

Lu, H., Hitchman, M.H., Gray, L.J., Anstey, J.A. and Osprey, S.M. (2020) On the role of Rossby wave breaking in the quasi-biennial modulation of the stratospheric polar vortex during boreal winter. *Quart J. Roy. Meteor. Soc*, 146, 1939–1959.

Marsh, D.R., Mills, M.J., Kinnison, D.E., Lamarque, J.-F., Calvo, N. and Polvani, L.M. (2013) Climate change from 1850 to 2005 simulated in CESM1 (WACCM). *Journal of Climate*, 26, 7372–7391. https://doi.org/10.1175/JCLI-D-12-00558.1.

Matsuno, T. (1970) Vertical propagation of stationary planetary waves in the winter northern hemisphere. *Journal of the Atmospheric Sciences*, 27, 871–883. https://doi.org/10.1175/1520-0469(1970)027<0871:VPOSPW>2.0.CO;2.

Matthes, K., Marsh, D.R., Garcia, R.R., Kinnison, D.E., Sassi, F. and Walters, S. (2010) Role of the QBO in modulating the influence of the 11 year solar cycle on the atmosphere using constant forcings. *Journal of Geophysical Research Atmospheres*, 115(D18). https://doi.org/10.1029/2009JD013020.

McIntyre, M.E. (1992) Atmospheric dynamics: some fundamentals, with observational implications. *The use of EOS for studies of atmospheric Physics*, 313, 342–357.

McIntyre, M.E. and Palmer, T.N. (1985) A note on the general concept of wave breaking for Rossby and gravity waves. *Pure and Applied Geophysics*, 123, 964–975. https://doi.org/10.1007/BF00876984.

Naito, Y. and Yoden, S. (2006) Behavior of planetary waves before and after stratospheric sudden warming events in several phases of the equatorial QBO. *Journal of the Atmospheric Sciences*, 63, 1637–1649. https://doi.org/10.1175/1520-0469(2003)060<1380:APSEOT>2.0.CO;2.

Nakamura, H., Nakamura, M. and Anderson, J.L. (1997) The role of high- and low-frequency dynamics in blocking formation. *Mon. Weather Rev.*, 125, 2074–2093. https://doi.org/10.1175/1520-0493(1997)125<2074:TROHAL>2.0.CO;2.

Naoe, H. and Shibata, K. (2010) Equatorial quasi-biennial oscillation influence on northern winter extratropical circulation. *Journal of Geophysical Research*, 115(D19). https://doi.org/10.1029/2009JD012952.

O'Neill, A. and Pope, V.D. (1988) Simulations of linear and non-linear disturbances in the stratosphere. *Quarterly Journal of the Royal Meteorological Society*, 114, 1063–1110. https://doi.org/10.1002/qj.49711448210.

Peings, Y. (2019) Ural blocking as a driver of early-winter stratospheric Warmings. *Geophys.Res. Lett.*, 46, 5460–5468. https://doi.org/10.1029/2019GL082097.

Peña-Ortiz, C., Ribera, P., García-Herrera, R., Giorgetta, M.A. and García, R.R. (2008) Forcing mechanism of the seasonally asymmetric quasi-biennial oscillation secondary circulation in ERA-40 and MAECHAM5. *Journal of Geophysical Research: Atmospheres*, 113(D16). https://doi.org/10.1029/2007JD009288.

Plumb, R. (1985) On the three-dimensional propagation of stationary waves. *Journal of the Atmospheric Sciences*, 42, 217–229. https://doi.org/10.1175/1520-0469(1985)042<0217:OTTDPO>2.0.CO;2.

Plumb, R.A. and Bell, R.C. (1982) A model of the quasi-biennial oscillation on an equatorial beta-plane. *Quarterly Journal of the Royal Meteorological Society*, 108, 335–352. https://doi.org/10.1256/smsqj.45603.

Rao, J., Garfinkel, C.I. and White, I.P. (2020) Impact of the Quasi-biennial oscillation on the northern winter stratospheric polar vortex in CMIP5/6 models. *Journal of Climate*, 33(11), 4787–4813.

Rayner, N.A., Parker, D.E., Horton, E.B., Folland, C.K., Alexander, L.V., Rowell, D.P., Kent, E.C. and Kaplan, A. (2003) Global analyses of sea surface temperature, sea ice, and night marine air temperature since the late nineteenth century. *Journal of Geophysical Research*, 108, 4407. https://doi.org/10.1029/2002JD002670.

Richter, J.H., Anstey, J.A., Butchart, N., Kawatani, Y., Meehl, G.A., Osprey, S. and Simpson, I.R. (2020) Progress in simulating the quasi-biennial oscillation in CMIP models. *Journal of Geophysical Research: Atmospheres*, 125(8). https://doi.org/10.1029/2019JD032362.

Ruzmaikin, A., Feynman, J., Jiang, X. and Yung, Y.L. (2005) Extratropical signature of the quasi-biennial oscillation. *Journal of Geophysical Research*, 110, D11111. https://doi.org/10.1029/2004JD005382.

Scott, R.K. and Haynes, P.H. (1998) Internal interannual variability of the extratropical stratospheric circulation: the low-latitude flywheel. *Quarterly Journal of the Royal Meteorological Society*, 124, 2149–2173. https://doi.org/10.1002/qj.49712455016.

Silverman, V.N., Harnik, K., Matthes, S.W.L. and Wahl, S. (2018) Radiative effects of ozone waves on the northern hemisphere polar vortex and its modulation by the QBO. *Atmospheric Chemistry and Physics*, 18, 6637–6659. https://doi.org/10.5194/acp-18-6637-2018.

Simpson, I.R., Blackburn, M. and Haigh, J.D. (2009) The role of eddies in driving the tropospheric response to stratospheric heating perturbations. *Journal of the Atmospheric Sciences*, 66, 1347–1365. https://doi.org/10.1175/2008JAS2758.1.

Simpson, I.R., Blackburn, M. and Haigh, J.D. (2012) A mechanism for the effect of tropospheric jet structure on the annular mode–like

response to stratospheric forcing. *Journal of the Atmospheric Sciences*, 69, 2152–2170. https://doi.org/10.1175/JAS-D-11-0188.1.

Smith, D.M., Screen, J.A., Deser, C., Cohen, J., Fyfe, J.C., García-Serrano, J., Jung, T., Kattsov, V., Matei, D., Msadek, R., Peings, Y., Sigmond, M., Ukita, J., Yoon, J.-H. and Zhang, X. (2019) The polar amplification model Intercomparison project (PAMIP) contribution to CMIP6: investigating the causes and consequences of polar amplification. *Geoscientific Model Development Discussion*, 12(3), 1139–1164. https://doi.org/10.5194/gmd-2018-82.

Smith, K., Neely, R., Marsh, D. and Polvani, L. (2014) The specified chemistry whole atmosphere community climate model (SC-WACCM). *Journal of Advances in Modeling Earth Systems*, 6, 883–901. https://doi.org/10.1002/2014MS000346.

Tegtmeier, S., Anstey, J., Davis, S., Ivanciu, I., Jia, Y., McPhee, D. and Pilch Kedzierski, R. (2020) Zonal asymmetry of the QBO temperature signal in the tropical tropopause region. *Geophysical Research Letters*, 47(24). https://doi.org/10.1029/2020GL089533.

Thompson, D.W.J. and Wallace, J.M. (1998) The Arctic oscillation signature in the wintertime geopotential height and temperature fields. *Geophysical Research Letters*, 25, 1297–1300. https://doi.org/10.1029/98GL00950.

Wang, J., Kim, H.M. and Chang, E.K. (2018) Interannual modulation of northern hemisphere winter storm tracks by the QBO. *Geophysical Research Letters*, 45, 2786–2794. https://doi.org/10.1002/2017GL076929.

White, I., Garfinkel, C.I., Gerber, E.P., Jucker, M., Aquila, V. and Oman, L.D. (2019) The downward influence of sudden stratospheric warmings: association with tropospheric precursors. *Journal of Climate*, 32, 85–108. https://doi.org/10.1175/JCLI-D-18-0053.1.

White, I.P., Lu, H. and Mitchell, N.J. (2016) Seasonal evolution of the QBO-induced wave forcing and circulation anomalies in the northern winter stratosphere. *Journal of Geophysical Research: Atmospheres*, 121, 10 411–10 431. https://doi.org/10.1002/2015JD024507.

White, I.P., Lu, H., Mitchell, N.J. and Phillips, T. (2015) Dynamical response to the QBO in the northern winter stratosphere: signatures in wave forcing and eddy fluxes of potential vorticity. *Journal of the Atmospheric Sciences*, 72, 4487–4507. https://doi.org/10.1175/JAS-D-14-0358.1.

White, R.H., Battisti, D.S. and Roe, G.H. (2017) Mongolian mountains matter most: impacts of the latitude and height of Asian orography on Pacific wintertime atmospheric circulation. *Journal of Climate*, 30, 4065–4082. https://doi.org/10.1175/JCLI-D-16-0401.1.

Yamashita, Y., Akiyoshi, H. and Takahashi, M. (2011) Dynamical response in the northern hemisphere midlatitude and high-latitude winter to the QBO simulated by CCSR/NIES CCM. *Journal of Geophysical Research*, 116(D6). https://doi.org/10.1029/2010JD015016.

Zhang, J., Xie, F., Ma, Z., Zhang, C., Xu, M., Wang, T. and Zhang, R. (2019) Seasonal evolution of the quasi-biennial oscillation impact on the northern hemisphere polar vortex in winter. *Journal of Geophysical Research: Atmospheres*, 124(23), 12568–12586. https://doi.org/10.1029/2019JD030966.

Zhang, J.L. and Rothrock, D.A. (2003) Modeling global sea ice with a thickness and enthalpy distribution model in generalized curvilinear coordinates. *Monthly Weather Review*, 131, 845–861. https://doi.org/10.1175/1520-0493(2003)131<0845:MGSIWA>2.0.CO;2.

SUPPORTING INFORMATION

Additional supporting information may be found online in the Supporting Information section at the end of this article.